**Carbon mineralization in Laptev and East Siberian Sea shelf and slope sediment**

Volker Brüchert[1,3], Lisa Bröder[2,3], Joanna E. Sawicka[1,3], Tommaso Tesi[2,3,5], Samantha P. Joye[6], Xiaole Sun[4,5], Igor P. Semiletov[7,8,9], Vladimir A. Samarkin[6]

[1] Department of Geological Sciences, Stockholm University, Stockholm, Sweden

[2] Department of Environmental Sciences and Analytical Chemistry, Stockholm University, Stockholm, Sweden

[3] Bolin Centre for Climate Research, Stockholm University, Stockholm, Sweden

[4] Baltic Sea Research Center, Stockholm University, Stockholm, Sweden

[5] Institute of Marine Sciences – National Research Council, Bologna, Italy

[6] Department of Marine Sciences, University of Georgia, Athens, U.S.A.

[7] International Arctic Research Center, University Alaska Fairbanks, Fairbanks, USA

[8] Pacific Oceanological Institute, Russian Academy of Sciences, Vladivostok, Russia

[9] Tomsk National Research Politechnical University, Tomsk, Russia

**Abstract** The Siberian Arctic Sea shelf and slope is a key region for the degradation of terrestrial organic material transported from the organic carbon-rich permafrost regions of Siberia. We report on sediment carbon mineralization rates based on $O_2$ microelectrode profiling, intact sediment core incubations, $^{35}S$-sulfate tracer experiments, porewater dissolved inorganic carbon (DIC), $\delta^{13}C_{DIC}$, and iron, manganese, and ammonium concentrations from 20 shelf and slope stations. This data set provides a spatial overview of sediment carbon mineralization rates and pathways over large parts of the outer Laptev and East Siberian Arctic shelf and slope and allowed us to assess degradation rates and efficiency of carbon burial in these sediments. Rates of oxygen uptake and iron and manganese reduction were comparable to temperate shelf and slope environments, but bacterial sulfate reduction rates were comparatively low. In the topmost 50 cm of sediment, aerobic carbon mineralization dominated degradation and comprised on average 84% of the depth-integrated carbon mineralization. Oxygen uptake rates and anaerobic carbon mineralization rates were higher in the eastern East Siberian Sea shelf compared to the Laptev Sea shelf. DIC/$NH_4^+$ ratios in porewaters and the stable carbon isotope composition of remineralized DIC indicated that the degraded organic matter on the Siberian shelf and slope was a mixture of marine and

terrestrial organic matter. Based on dual end member calculations, the terrestrial organic carbon contribution varied between 32% and 36%, with a higher contribution in the Laptev Sea than in the East Siberian Sea. Extrapolation of the measured degradation rates using isotope end member apportionment over the outer shelf of the Laptev and East Siberian Sea suggests that about 16 Tg C per year are respired in the outer shelf sea floor sediment. Of the organic matter buried below the oxygen penetration depth, between 0.6 and 1.3 Tg C per year are degraded by anaerobic processes, with a terrestrial organic carbon contribution ranging between 0.3 and 0.5 Tg per year.

Key words: Carbon mineralization, Arctic shelf and slope sediment, Laptev Sea, East Siberian Sea

## 1. Introduction

The biogeochemical fate of terrestrial organic carbon deposited on the Arctic shelf and slope is one of the most important open questions for the marine Arctic carbon cycle (e.g., Tesi et al., 2014; Macdonald et al., 2015; McGuire et al., 2009; Vonk et al, 2012). The total pan-Arctic terrestrial permafrost region has been estimated to contain about 1100 – 1500 Pg carbon, of which 500 Pg are seasonally or perennially unfrozen and contribute to the present-day carbon cycle (Hugelius et al, 2014). Additional partial thawing, mobilization, and oxidation of the perennially frozen carbon reservoir can substantially affect the global atmospheric carbon dioxide pool over the next 100 years (Schuur et al. 2015; Koven et al., 2015). A key problem in this context is the considerable uncertainty regarding the mineralization of terrestrial organic matter exported by rivers and coastal erosion to the Siberian shelf and slope (Tesi et al., 2014; Karlsson et al. 2015; Semiletov et al., 2011; Salvado et al., 2016).

Terrestrial organic matter transported to the Siberian shelf is of variable size, age, and molecular composition, which results in a range of different carbon degradation rates of bulk carbon and individual molecular components. Size class analysis of the organic matter suggests that coarse organic material settles preferentially in near-shore environments, whereas finer organic fractions disperse offshore in repeated deposition-resuspension cycles gradually losing particular molecular components and overall reactivity (Wegner et al., 2013; Tesi et al., 2014, 2016). Substantial oxic degradation of organic matter may occur during

near-bottom transport in resuspension-deposition cycles across the shelf (Bröder et al., 2016a). Up to 90% of certain biomarker classes may decompose during transport, whereby most of the degradation may take place while the transported organic material resides in the sediment before being resuspended (Bröder et al., 2016a). However, without making approximations on transport direction, particle travel time and travel distance these studies cannot provide direct insights into the rates of carbon degradation and resultant $CO_2$ fluxes from sediment. By contrast, direct kinetic constraints provided by sediment carbon degradation rates can provide testable data for coupled hydrodynamic biogeochemical models that help assess the fate of land-exported terrestrial carbon pool on the Siberian shelf.

Relatively few studies have directly measured rates of carbon mineralization in Siberian shelf sediment (e.g., Boetius and Damm, 1998; Grebmeier et al., 2006; Karlsson et al., 2015, Savvichev et al., 2007). Boetius and Damm (1998) used high-resolution oxygen microelectrode data to determine the surface oxygen concentration gradients and oxygen penetration depths in a large number of sediment cores from the shelf and slope of the Laptev Sea. Based on corresponding sediment trap and export productivity data, they concluded that the annual marine organic carbon export in the Laptev Sea shelf and slope was sufficiently high to explain the observed oxygen uptake rates. Current understanding therefore holds that due to the long annual ice cover and low productivity on the eastern Siberian Arctic shelf and slope, only a small amount of marine organic carbon is exported and buried in Laptev and East Siberian Sea shelf sediment. The highly reactive fraction of fresh organic matter is thought to degrade in the surface sediment (Boetius and Damm, 1998). Consequently, anaerobic respiration in buried sediment has been thought to be negligible and to reflect the degradation of unreactive terrestrially derived carbon compounds. To our knowledge, with the exception of a recent study by Karlsson et al (2015) a more direct assessment of terrestrial carbon-derived mineralization rates in buried shelf and slope sediment has not been reported for the East Siberian Arctic Sea.

In this study, we present data from oxygen microelectrode profiling experiments, porewater data of dissolved inorganic carbon and its stable carbon isotope composition, and $^{35}$S-sulfate reduction rate experiments along a shelf-slope transect near 125°E in the Laptev Sea. Samples were taken during the summer 2014 on the SWERUS-C3 expedition with the Swedish icebreaker Oden. We combined these data with porewater analyses of dissolved ammonium, sulfate, iron, and manganese to assess the major carbon degradation pathways and rates across the extensive outer Laptev and Siberian shelf and slope.

## 2. Materials and methods

### 2.1. Sample collection

Samples were collected at 20 stations from 40 to 3146 m water depth in the western Laptev and East Siberian Sea (Fig. 1 and Table 1). In this study we only report on sampling sites that showed no methane gas plumes, acoustic anomalies in the water column, or sediment blankings indicative of rising gas. In areas of active ebullition from the seafloor as seen by video imagery and acoustic gas blankings in the water column, the biogeochemistry of sea floor processes such as bacterial sulfate reduction, DIC concentration and its carbon isotope composition, and oxygen uptake are affected by methane oxidation. These methane cycling-related signals overprint the biogeochemistry imparted by carbon mineralization and are reported in a separate study.

Sediment stations had variable ice cover (Table 1). In the Laptev Sea, except for the deep-water slope stations between 3146 m and 2106m, all stations had open water. By contrast, ice cover exceeded 75% in the East Siberian Sea to the west and east of Bennett island (Station 40 to 63). Sediments with well-preserved sediment surfaces were collected with a Multicorer (Oktopus GmbH, Kiel, Germany) that simultaneously takes 8 sediment cores over an area of about 0.36 m$^2$ with acrylic tubes (9.5 cm diameter, 60 cm length) to 40 cm depth preserving clear water on top of the sediment. At stations 6, 23, and 24, an underwater video system (Group B Distribution Inc., Jensen Beach, U.S.A.) was mounted on the multicore frame to record the deployment and recovery, and to document the sea floor habitat. For the analyses all cores were taken from the same cast. Two of the cores were used to determine $^{35}$S-sulfate reduction rates and porosity. In addition, one core with predrilled 3.8 mm holes sealed with electric tape was used to extract porewaters with rhizons (Rhizosphere Research Products BV, Wageningen, Netherlands). A fourth core was used for microelectrode measurements of dissolved oxygen concentration profiling, and finally, four other cores were used for whole-core incubations to determine benthic fluxes of dissolved oxygen, dissolved inorganic carbon, and nutrients. The cores were capped with rubber stoppers until further subsampling usually within 30 minutes. For sulfate reduction rates, the cores were subsampled with 40 or 50 cm long acrylic tubes (26 mm inner diameter) prepared with silicon-sealed holes, drilled at distances of 1 cm. For whole-core incubations, the cores were sub-sampled with 25 cm-long, 60 mm-wide tubes (56 mm id) to 12 cm depth. Likewise, a 60 mm diameter tube (56 mm id) was collected for microelectrode measurements preserving

129   about 3 cm of the overlying bottom water. For intact whole-core incubations, temperature-

130   controlled aquaria were filled with bottom water that was collected from a CTD rosette from

131   the same station by collecting water from four ten-liter rosette bottles usually ~5 meters above

132   the sea floor. All sediment cores were closed with a stopper retaining the water on top of the

133   sediment and stored at 1.5°C in an incubator until further processing.

134

135   **2.2. Microelectrode oxygen profiles**

136       High-resolution $O_2$-profiles across the water-sediment interface were obtained to

137   determine oxygen penetration depths and diffusive oxygen uptake (Rasmussen and Jørgensen,

138   1992; Glud, 2008) (Table 2). The 60 mm tubes were placed in an aquarium filled with bottom

139   water from the same station, overflowing the sediment core. The water temperature was kept

140   to ~1°C by a cooling unit (Julabo GmbH, Seelbach, Germany). In exceptional cases when

141   there was not sufficient bottom water available to fill the aquarium, bottom water was used

142   from a pump system. A stable diffusive boundary layer above the sediment was created by

143   passing air from an aquarium pump over the water surface with a Pasteur pipette creating a

144   slow rotational motion of water inside the core. At each station six to eight $O_2$ microprofiles

145   were measured using Clark-type oxygen microelectrodes (OX-50, Unisense, Århus Denmark)

146   mounted on a motor-driven micromanipulator (MM33, Unisense, Århus Denmark). $O_2$

147   sensors were calibrated with fully oxygenated bottom water from the same station at ~1°C for

148   saturation and for anoxic conditions by dissolving $Na_2SO_3$ in the same water. The first profile

149   in each core was measured with a resolution of 1000µm as a quick scan to locate the sediment

150   surface and to adjust the measuring range. Then the vertical resolution was increased to 100-

151   500µm and additional five to seven profiles were measured at different points on the surface,

152   approximately one cm apart from each other.

153

154   **2.3. Whole-core sediment incubations**

155       Four intact cores with clear overlying water were subsampled in the laboratory in

156   acrylic tubes (i.d. 56 mm, height 25 cm) retaining about 10 cm of the overlying water. The

157   sediment and water height in the tubes were approximately 10 cm. The cores were incubated

158   in a 40-liter incubation tank filled with bottom water from the same station. Before the

159   incubation the overlying water in the cores was equilibrated with bottom water in the tank.

160   The overlying water in the cores was stirred by small magnetic bars mounted in the core liners

161   and driven by an external magnet at 60 rpm. The cores were pre-incubated uncapped for 6

162   hours and subsequently capped and incubated for a period of 6 to 24 hours depending on the

163   initial oxygen concentration in the bottom water. 2D oxygen sensor spots (Firesting oxygen

164   optode, PyroScience GmbH, Aachen, Germany) with a sensing surface of a diameter of 5 mm

165   were attached to the inner wall of two incubation cores. The sensor spots were calibrated

166   against $O_2$-saturated bottom water and oxygen-free water following the manufacturer's

167   guidelines accounting for temperature and salinity of the incubation water. Measurements

168   were performed with a fiberoptic cable connected to the spot adapter fixed at the outer core

169   liner wall at the spot position. The $O_2$ concentration was continuously logged during

170   incubations. Sediment total oxygen uptake (TOU) rates were computed by linear regression of

171   the $O_2$ concentration over time. 5 ml of overlying water were removed over the course of the

172   incubation used for dissolved inorganic carbon (DIC) analysis as described below. Linear

173   regression best fits were used to determine the exchange fluxes of DIC.

174

175   **2.4. Extracted porewater analysis**

176   Porewater samples for concentration measurements of DIC, sulfate ($SO_4^{2-}$), and

177   ammonium ($NH_4^+$) were obtained using the methods described in Seeberg-Elverfeldt et al.

178   (2005). Rhizons were treated for 2 hours in 10% HCl solution, followed by two rinses with

179   deionized water for 2 hours and final storage in deionized water. The rhizons were connected

180   to 10 mL disposable plastic syringes with inert pistons (VWR, Stockholm, Sweden) via

181   polyethylene 3-way luer-type stopcocks (Cole-Parmer, U.S.A.) and inserted in 1-cm intervals

182   through tight-fitting, pre-drilled holes in the liner of the sediment cores. The first mL of pore

183   water was discarded from the syringe. No more than 5 ml were collected from each core to

184   prevent cross-contamination of adjacent porewater due to the suction effect (Seeberg-

185   Elverfeldt et al., 2005). The collected porewater was divided into four different aliquots for

186   later chemical analysis. For dissolved sulfate analysis, 1 ml of porewater was preserved with

187   200 µl of 5% zinc acetate solution and frozen. For ICP-AES analysis of dissolved metals and

188   major cations, 1 ml of porewater was preserved with 100 µl of 10% Suprapur $HNO_3$ and

189   stored cold. For analysis of dissolved ammonium, 2 ml of porewater were frozen untreated.

190   For analysis of DIC, 2 ml of porewater were preserved with 100 µl 10% $HgCl_2$ and stored

191   cold in brown glass vials without headspace. Ammonium was determined on a QUAATRO 4-

channel flow injection analyzer (Seal Analytical) on board.  All other porewater analyses were performed at the Department of Geological Sciences, Stockholm University. Samples that were analyzed in the home laboratory remained cold or frozen on board until arrival of the icebreaker Oden in Sweden. Sulfate concentration was measured on diluted aliquots on a Dionex System IC 20 ion chromatograph. DIC concentrations were determined by flow injection analysis (Hall and Aller, 1992).  Dissolved iron and manganese were determined on diluted aliquots by ICP-AES (Varian Vista AX). For carbon isotope analysis of dissolved inorganic carbon, 1 ml of porewater was filled into 12 ml exetainers to which 1 ml of concentrated phosphoric acid was added. The carbon isotope composition of the formed $CO_2$ was analyzed on a GasbenchII-MAT 253 isotope ratio mass spectrometer coupled to a GC-PAL autosampler. Results are reported in the conventional delta notation relative to PDB. Precision of isotope analysis is 0.1‰.

For the calculation of porewater concentration ratios of DIC and $NH_4^+$, the effects of different diffusion coefficients and ammonium adsorption were accounted for. We have no direct measurements of adsorption coefficients for these sediments. Instead, we used an ammonium adsorption coefficient of 1.3 established for comparable, terrestrially dominated silty clays in the East China Sea for which similar porosities and organic carbon concentrations were reported (Mackin and Aller, 1984). The diffusion coefficient of $HCO_3^-$ is about 45% smaller than the diffusion coefficient of $NH_4^+$ (Li and Gregory, 1974). The two effects required an upward correction of the ammonium concentration by 40% to facilitate direct comparison in DIC/$NH_4^+$ ratios. Diffusion- and adsorption-adjusted DIC/$NH_4^+$ ratios were also corrected for the bottom water DIC and $NH_4^+$ concentrations (Table 1). Only concentrations below 4 cm depth were used for comparison to avoid effects of oxidation on $NH_4^+$ concentrations.

## 2.5. Reaction transport modelling

Reaction rates and fluxes were estimated from the concentration profiles of dissolved oxygen, manganese, iron, and dissolved inorganic carbon according to the general reaction-transport equation at steady state accounting for diffusion and advection described here for dissolved oxygen according to

$$\frac{d}{dz} = \left( \varphi (D_s + D_b) \frac{dO_2}{dz} \right) + \varphi \alpha \left( O_{2,\ z=0} - O_{2,\ z} \right) + \sum R = 0$$

(1)

223     At steady state, the rate of the concentration change reflects the balance between the

224     consumption due to respiration and oxidation of reduced inorganic compounds (R) against

225     diffusion and advection due to bioirrigation into sediment (Glud, 2008). $D_s$ ($cm^2 s^{-1}$) is the

226     sediment diffusion coefficient and was calculated for the experimental temperature and

227     salinity according to Boudreau (1997). The sediment diffusion coefficient $D_s$ was recalculated

228     from the molecular diffusion coefficient $D_o$ according to $D_s = D_o / \theta^2$, where $\theta^2 = 1 - \ln(\varphi^2)$,

229     where $\varphi$ is porosity and $\theta$ is tortuosity (Boudreau, 1997). $D_b$ ($cm^2 s^{-1}$) is the bioturbation

230     coefficient and $\alpha$ is the irrigation coefficient ($cm s^{-1}$). $D_b$ and $\alpha$ were estimated by stepwise

231     optimization by fitting a concentration profile to the measured data using the least square

232     fitting procedure of the program Profile (Berg et al., 1998) testing various coefficients until

233     the statistically best fit was obtained. Boundary conditions and the coefficients $D_b$ and $\alpha$ for

234     the best fits are shown in the supplemental material Table 1.

235

236     **2.6. $^{35}$S-Sulfate reduction rates ($^{35}$SRR)**

237     For the incubations, the whole-core incubation method by Jørgensen (1978) was used.

238     $^{35}SO_4^{2-}$ tracer solution was diluted in a 6 ‰ NaCl solution containing 0.5 mM $SO_4^{2-}$ and 2.5 µl

239     of the tracer solution (200kBq) was injected through the pre-drilled holes. The cores were

240     then capped and sealed in plastic wrap foil and incubated for 8 hours at the respective bottom

241     water temperatures. After this time, the incubations were stopped by sectioning the core in 1-

242     cm intervals to 5 cm depth and in two centimeter intervals below this depth to the bottom of

243     the core. Sediment sections were transferred into 50 ml plastic centrifuge tubes containing 20

244     ml zinc acetate (20% v/v), mixed to a slurry on a vortex stirrer and frozen. The total amount

245     of $^{35}$S-labeled reduced inorganic sulfur (TRIS) was determined using the single-step cold

246     chromium distillation method by Kallmeyer et al. (2004). TRIS and supernatant sulfate were

247     counted on a TriCarb 2095 Perkin Elmer scintillation counter. The sulfate reduction rate was

248     calculated using the following equation (Jørgensen, 1978):

249     $$^{35}SRR = \left( {TRI^{35}S \times 1.045} \Big/ {(^{35}SO_4^{2-} + TRI^{35}S)} \right) \times [SO_4^{2-}]/\rho T \qquad (2)$$

250     where [$SO_4^{2-}$] is the pore water sulfate concentration corrected for porosity $\rho$, TRI$^{35}$S and

251     $^{35}SO_4^{2-}$ are the measured counts (cpm) of sulfate and total reduced inorganic sulfur species,

252     respectively, 1.045 is a correction factor accounting for the kinetic isotope effect of $^{35}$S

253 relative to $^{32}$S, and T is the incubation time. The sulfate reduction rate is reported as nmol cm$^-$

254 $^3$ day$^{-1}$. $^{35}$SRR were measured in two parallel cores for all depth intervals. The incubation

255 experiments were conducted between July 15 and August 20, but for logistical reasons

256 (transport to Stockholm) the distillation of the samples was conducted between December 10,

257 2014 and April 2, 2015 so that between 1.7 and 2.7 half-lives of $^{35}$S (87.4 days) had passed

258 before all samples were processed. The resulting detection limit of the rate measurements

259 accounting for distillation blanks and radioactive decay of $^{35}$S between experiment and

260 laboratory workup was 0.01 nmol cm$^{-3}$ day$^{-1}$.

261

262 **2.7. Carbon equivalent apportionment of terminal electron-accepting processes**

263 The modelled oxygen, iron, manganese, and DIC reaction rates were integrated over 30 cm

264 sediment depth to permit comparison between different stations. The integrated terminal

265 electron accepting processes (TEAP) were recalculated into carbon equivalents for the

266 electron acceptors oxygen, iron, manganese, and sulfate using an idealized $(CH_2O)_x$

267 stoichiometry for organic matter (Vandieken et al., 2006; Nickel et al., 2008). The calculated

268 rates were then used to calculate the contribution of the different aerobic and anaerobic

269 electron acceptors to total carbon mineralization for 5 stations in the Laptev and East Siberian

270 Sea (Table 3).

271

272 **2.8 Marine versus terrestrial endmember partitioning of carbon degradation rates**

273 In order to determine the proportion of mineralized terrestrial and marine organic

274 matter in porewater DIC, we used a two-endmember isotope mass balance model. Porewater

275 DIC is assumed to be derived from bottom-water DIC and remineralization of organic matter

276 during burial. We used a Keeling-type plot of 1/DIC against the corresponding stable carbon

277 isotope composition of DIC to determine the isotope composition of the remineralized

278 endmember by linear regression (Fig. 5b). The method assumes that diffusion is slow

279 compared to burial and mineralization and that isotope fractionation during the oxidation of

280 organic matter is negligible. Removal or addition of DIC by diagenetic processes such as

281 $CaCO_3$ precipitation or dissolution were minor. This is supported by the observation that the

282 porewater concentrations of $Ca^{2+}$ and $Mg^{2+}$ at these shelf and slope stations did not change

283 significantly with depth (Brüchert and Sun, unpubl. data). The relative contribution of the

284 terrestrial and marine organic carbon was calculated with a linear two-endmember isotope

285 model:

286 $\delta^{13}C_{DIC, \text{remineralized}} = f_{terr} * \delta^{13}C_{terr\ OC} + f_{mar} * \delta^{13}C_{marine\ OC}$          (4)

287 where $f_{terr}$ and $f_{mar}$ are the respective mass fractions of terrestrial and marine-derived organic

288 carbon and $\delta^{13}C_{terr\ OC}$ and $\delta^{13}C_{marine\ OC}$ reflect the isotope composition of these endmembers.

289 For the Laptev Sea shelf, a fraction of the surface water DIC used for marine production is

290 derived from terrestrial DOC and POC remineralized in shelf waters and transported from

291 land (Humborg et al., 2017; Tesi et al., 2017; Alling et al., 2012). $\delta^{13}C$ values of offshore

292 sediment in the Laptev Sea sediment are as heavy as -22.3 ‰ (Salvado et al., 2016). Tesi et al

293 (2017) report $\delta^{13}C$ of POC of -24.7 ‰ for outer Laptev Sea POC near the ice edge containing

294 abundant dinoflagellates and only trace indicators of terrestrial organic carbon. Based on these

295 data we use an isotope endmember composition of -23.0 ‰ for marine organic matter in the

296 Laptev Sea. We are aware that there may be regional variations in this endmember

297 composition. An isotope composition of -28 ‰ was used for the terrestrial organic carbon

298 contribution in the Laptev Sea (Vonk et al., 2012). For the East Siberian Sea east of 140°E,

299 the heaviest calculated isotope composition of remineralized porewater DIC was -19 ‰ and is

300 used here as the marine endmember (Station 53). The same carbon isotope composition of -28

301 ‰ as for the Laptev Sea was used as the terrestrial end member. In order to derive specific

302 degradation rates of the marine and terrestrial carbon fractions, the endmember mixing-based

303 assessment of the marine and terrestrial organic carbon contributions to DIC were combined

304 with the mineralization rates derived for the different electron acceptors.

305

306 **3. Results**

307 **3.1. Physical and chemical bottom water conditions**

308        Table 1 summarizes the general site characteristics of the investigated sediment

309 stations. Bottom water salinity varied between 34.9 ‰ in the outer Laptev Sea at 3146 m

310 depth (Station 1) to 29.1 ‰ in the East Siberian Sea at 40 m (Station 45). The lower salinity

311 in the East Siberian Sea can be attributed to longshore transport of freshwater eastward from

312 the Lena River. Bottom water temperatures varied between -1.8°C at Station 27 and 0°C at

313 Station 37, but there was no regional trend in the data. Cored sediment consisted of silty clays

to clayey silts. Slope sediment had a distinctly brown color throughout the cored interval, whereas shelf sediment only had a 1 to 4 cm-thick brown interval, below which the sediment color changed to grey. In the eastern part of the East Siberian Sea, the sediment was mottled black below 10 cm depth. Iron-manganese concretions were found between 2 cm and 10 cm depth at stations 24, 42, and 43, but were also observed at other stations on the shelf that were not part of this study. Benthic macrofauna, when present, consisted mainly of brittle stars, isopods, few polychaetes, and rare bivalves. All bottom waters were well-oxygenated with concentrations higher than 190 µmol/l, but the shelf bottom-waters in the East Siberian Sea had generally lower concentrations than in the Laptev Sea and bottom waters on the continental slope had lower oxygen concentrations than on the shelf. Concentrations of bottom-water ammonium ranged between 0.2 µmol/L and 1.8 µmol/L. Generally, the slope stations and the shelf stations nearest to the Lena delta had the highest ammonium concentrations, whereas the other shelf stations showed no clear regional trend other than proximity to the Lena delta. Bottom water DIC concentrations varied between 2086 µM (Station 53) and 2598 µM (Station 27), and the stable carbon isotope composition of DIC in the waters overlying the cores were between -0.5 ‰ and -6.5 ‰ vs. VPDB.

## 3.2. Dissolved oxygen, manganese, and iron

We show representative profiles of oxygen concentrations in Figure 2 for the Laptev Sea slope station 1, the Laptev Sea shelf stations 23, 30, 45, and the East Siberian Shelf Sea 53 and 63. Oxygen penetration depths varied between 3 mm at Station 58 and more than 60 mm in all slope sediments (Table 2). For the Laptev Sea slope stations 1, 2, 3, and 4, the maximum depth of oxygen penetration could not be determined, because at penetration greater than 60 mm the conical sensor needle opened a hole in the sediment through which oxygen-containing bottom water could potentially have entered the sediment at depth thereby artificially extending the oxygen penetration depth. In the slope-to-shelf transects the oxygen penetration depth decreased from >60 mm off-shore to 10 mm at the most inshore station in the Laptev Sea and the East Siberian Sea. At the two easternmost shelf stations 58 and 63, we measured the lowest oxygen penetrations depths, 3 mm and 4 mm, respectively. Evidence for bioturbation and bioirrigation based on multiple microelectrode profile measurements per core was rare. Only at Station 48 a clear increase in oxygen concentrations below the sediment surface was observed, indicative of active bioirrigating macrofauna. However, even

346 at this station, based on investigations in parallel multicore casts, fauna was not abundant (A.

347 Gukov, pers. comm.). At all other stations, oxygen concentrations decreased exponentially

348 with depth. Fitting of the oxygen concentration profiles to the steady advection-diffusion-

349 transport model (Eq. 1) yielded fluxes that varied between 0.81 and 11.49 mmol $m^{-2}$ $d^{-1}$

350 (Table 2). These calculated $O_2$ fluxes compared well with total oxygen uptake rates calculated

351 from whole-core incubations using 2D optode sensor spots (Table 2). The good fit between

352 the two methods also supports the notion that bioirrigation and bioturbation effects from

353 meiofauna and macrofauna were minor.

354        In the slope sediment at Station 1, concentrations of dissolved manganese and iron

355 were low throughout the cored depth interval and below 0.2 and 0.5 µM, respectively. The

356 exception was a small increase for both elements between 4 and 8 cm depth and 14 and 20 cm

357 depth to concentrations of less than 3 µM, possibly due to slightly more degradable organic

358 material in these depth intervals (Fig. 2). A similar concentration profile was found for the

359 other slope station 4 (data not shown), but here concentrations were below 2 µM throughout

360 for both dissolved iron and manganese and only slightly higher in the topmost cm. On the

361 shelf, in the Laptev Sea (Station 23 and 30), concentrations of dissolved manganese and iron

362 were below 0.3 µM and 1.5 µM, respectively, in the top 2 cm and 3 cm at Station 23, before

363 increasing to maximum concentrations of 69 and 134 µM. At both stations, metal

364 concentrations decreased again below the concentration maximum indicating that deeper

365 buried sediment was not a source of the metals and that the dominant source of iron and

366 manganese was reduction in the topmost 5 cm of sediment. There was a general trend of

367 increasing manganese concentrations from west to the east. At Station 30 in the Laptev Sea,

368 the concentration of dissolved manganese was less than 0.3 µM in the topmost cm, but

369 increased steeply to maximum concentrations of 189 µM at 9 cm depth. Similarly, dissolved

370 iron concentrations were below 1 µM to 4 cm depth and then increased to 144 µM. Again,

371 below the maximum, both iron and manganese porewater concentrations decreased with

372 increasing sediment depth. Even higher iron and manganese concentrations were found in the

373 East Siberian Sea (Stations 45, 53, 63), where dissolved manganese already increased from

374 the bottom water to concentrations of 20 µM in the topmost centimeter of sediment, and iron

375 increased to above 1 µM below 2 cm depth. The steepest manganese concentration gradient

376 was found at Station 63 in the easternmost East Siberian Sea, where concentrations were 501

377 µM in the first cm of sediment with a concentration maximum of 548 µM at 2.5 cm depth

378 decreasing below this depth to 115 µM at 30 cm depth. Station 63 differed with respect to

379  dissolved iron concentrations from the other stations, because here dissolved iron showed two

380  small peaks at 3.5 cm and 7 cm, and concentration increased substantially only below 17 cm

381  depth to concentrations of 189 µM.

382

### 3.3. $^{35}$S-sulfate reduction rates and porewater sulfate

384     Sulfate concentrations showed minor depth gradients at all sampling sites (Fig. 3) and

385  decreased from starting concentrations between 23.9 mM and 28.1 mM by 0.4 mM to 2.5 mM

386  from the top to the bottom of the cores. At all stations, turnover of $^{35}$S-tracer was recorded

387  from the topmost sediment interval to the bottom of the core indicating active bacterial sulfate

388  reduction (Fig. 3). Depth-integrated rates over the recovered core lengths varied between 0.03

389  and 1.41 mmol m$^{-2}$ d$^{-1}$ (Table 2). The integrated rates were lowest at Station 1 at 3146 m in

390  the Laptev Sea and highest at the Station 63 in the easternmost East Siberian Sea. Across the

391  shelf (Stations 6 to 24), depth-integrated rates increased from the west to the east. Examples

392  of sulfate reduction profiles are shown in Fig. 3 for the same six stations as previously. At

393  Station 1, these rates ranged from 0.03 to 0.38 nmol cm$^{-3}$ d$^{-1}$. At this station, the variability

394  between replicate cores was large, likely because many rates were near the detection limit in

395  our handling procedure. Overall, sulfate reduction was higher in the top 10 cm of sediment,

396  but showed no pronounced change with depth at this station. This suggests that the reactivity

397  of the organic material did not change substantially over the cored depth interval. The second

398  slope station, Station 4, showed a similar rate-depth profile than Station 1. Depth profiles for

399  the mid-outer shelf stations 23 to 63 all showed broad sub-surface maxima between 2.5 and

400  17.5 cm, but the depths of the rate maxima differed between the different stations (Fig. 3).

401  Peak rates varied between 0.6 nmol cm$^{-3}$ d$^{-1}$ at Station 30 and 39 nmol cm$^{-3}$ d$^{-1}$ at Station 63.

402  The second highest rate, 7.6 nmol cm$^{-3}$ d$^{-1}$, was found at the station nearest to the Lena delta,

403  Station 23. At all stations, sulfate reduction rates decreased from the maxima to rates below 1

404  nmol cm$^{-3}$ d$^{-1}$ or below the detection limit at the bottom of the cores. A particularly sharp

405  decrease in the sulfate reduction rate was observed between 8 and 9 cm at Station 63, where

406  rates dropped from 8.5 to 0.1 nmol cm$^{-3}$ day$^{-1}$ over 1 cm depth. Since sulfate was abundant

407  throughout the cored intervals, this order-of-magnitude decrease indicates substantial changes

408  in the reactivity of buried organic matter. Although no abrupt change in grain size or organic

409  carbon was observed in this core, it is likely that a historical change in organic sedimentation

410  took place during deposition across this time interval.

**3.4. Porewater DIC, NH$_4^+$, and δ$^{13}$C$_{DIC}$**

Porewater concentrations of DIC and NH$_4^+$ increased with depth at all stations (Fig. 4). The increase of DIC was between 0.6 mM (Station 23) and 2.3 mM (Station 45) over the cored sediment depths. Ammonium concentrations increased between 16.8 µM (Station 1) and 549 µM (Station 50). The steepness of the depth gradients was consistent with the rates of oxygen uptake and bacterial sulfate reduction for the different stations. The porewater pattern at Station 63 was an exception, because this station had the highest oxygen uptake and the highest sulfate reduction rates of all stations, but showed only a modest increase in DIC and NH$_4^+$ concentrations by 1.5 mM and 57 µM, respectively, over the cored sediment depth. The low DIC concentrations are consistent with the very low rates of sulfate reduction below 10 cm depth. Since these deeper layers have not produced large amounts of DIC and NH$_4^+$, only the surface 10 cm contribute significantly to total carbon mineralization and ammonium production.

For the anoxic parts of the sediment, DIC/NH$_4^+$ ratios varied between 8.4 for Station 24 and 40 respectively for Stations 1 in the Laptev Sea, and between 7.2 and 18.8 in the East Siberian Sea, with an overall mean DIC/NH$_4$ ratio of 9.8 for all stations excluding the continental slope stations (Fig. 5a). The δ$^{13}$C values of DIC consistently decreased with sediment depth indicating the addition of $^{13}$C-depleted remineralized carbon to DIC. The greatest downcore depletion in $^{13}$C was observed at stations 45, 48, and 50, where δ$^{13}$C of DIC decreased from -2.0 ‰ near the sediment surface to -13.9, -16.4, and -18.6 ‰ at the bottom of the cores (Fig. 4).

**3.5. Benthic exchange and modelled O$_2$, iron, and manganese reduction rates**

Benthic exchange fluxes from whole-core incubations and modelled DIC fluxes are shown in Table 2. There was a good agreement between 2D O$_2$ optode flux measurements and modelled fluxes, whereas modelled DIC fluxes were generally lower than whole-core incubation fluxes. We attribute this discrepancy to an underestimation of the DIC gradient at the sediment-water interface. Examples of the reaction transport modelling results for dissolved O$_2$, iron, and manganese are shown in Fig. 6 (Station 23). Optimal fits of the concentration profiles required a bioirrigation coefficient of 1 x 10$^{-4}$ cm$^2$ sec$^{-1}$ in the topmost 2 cm of sediment at Stations 23 and 53. For the other stations, optimal fits required no sediment

442    mixing by bioturbation or advective porewater transport by bioirrigation. This is consistent

443    with the low numbers of bioturbating macrofauna in the outer shelf sediment. $O_2$ consumption

444    rates exceeded sulfate and net reduction rates of iron and manganese by a factor of 100 (Fig.

445    6). On the shelf, most of the carbon oxidation therefore takes place in the topmost 5 mm. The

446    reaction rate depth profiles for iron and manganese indicate that manganese reduction

447    dominates in the topmost 2 cm of sediment followed by co-existing iron and sulfate reduction

448    below (Fig.6). Bacterial sulfate reduction was detected at a depth where the sediment was still

449    brown indicating abundant iron and manganese hydroxides. The modelled negative iron

450    production rates at the sediment surface indicate net iron oxidation by oxygen in the mixed

451    upper sediment layer. This pattern was not observed for manganese, which is consistent with

452    incomplete manganese oxidation at the sediment surface and loss of dissolved manganese to

453    the bottom water.

454

455    **4. Discussion**

456    **4.1 Coupled terminal electron-accepting processes**

457    The modelled efflux of manganese to the bottom water on the eastern Siberian Sea shelf

458    supports results by Macdonald and Gobeil (2012) that Arctic shelf sediments export dissolved

459    manganese to seawater and to the Arctic interior. Coexistence of net iron reduction and sulfate

460    reduction at the same depths make it difficult to quantify how much of the iron reduction is

461    coupled to heterotrophic carbon oxidation as opposed to the re-oxidation of sulfide produced

462    from bacterial sulfate reduction. The presence of dissolved iron throughout the measured

463    porewater profiles implies that iron reduction exceeded concomitant sulfate reduction, iron

464    sulfide precipitation, and reoxidation reactions, which supports the assessment of net

465    heterotrophic iron reduction. Assuming minor direct redox coupling between the terminal

466    electron-accepting processes, manganese and iron reduction contributed maximally between

467    2.3 and 23.7% to the total anaerobic carbon mineralization and between 0.3 and 2.3% to the

468    total carbon mineralization (Table 3). Even if our calculations only approximate the true

469    contribution of metals to carbon mineralization, the results indicate that bacterial sulfate

470    reduction is by far the major anaerobic carbon mineralization pathway in these sediments. The

471    prevalence of bacterial sulfate reduction in anaerobic carbon mineralization agrees with

472    results of Vandieken et al. (2006) and Nickel et al. (2008) from the northern Barents Sea

473    where ice-free stations support higher rates of sulfate reduction than the more permanently

474    ice-covered stations reflecting lower carbon export production.

475    The significant correlation ($r^2$ 0.75, P < 0.05) between the dissolved $O_2$ uptake and anaerobic

476    carbon degradation by sulfate reduction with a slope of 6.1±1.1 (Fig. 7) reflects the coupling

477    of oxygen uptake to the oxidation of reduced inorganic metabolites (FeS and $H_2S$) produced

478    during sulfate reduction (e.g., Glud, 2008; Jørgensen and Kasten, 2006; Thamdrup, 2000;

479    Berg et al., 2003). The percentage of the inverse of this slope, 16.4 %, is slightly lower than

480    the 23% reported for oxygenated coastal and continental shelf sediment (Canfield et al.,

481    2005), but is consistent with the notion that a substantial amount of the buried organic matter

482    in Siberian shelf sediment is oxidized anaerobically. The lower proportion of anaerobic

483    respiration compared to other shelf environments likely reflects the greater proportion of

484    highly reactive marine-derived organic material in the topmost millimeters of sediment.

485

## 4.2. Marine versus terrestrial organic matter contribution

487    Terrestrial organic carbon sources to the Laptev and East Siberian shelf and slope are

488    riverine discharge and coastal erosion of the ice core complex (Stein and Macdonald, 2004;

489    Vonk et al., 2012; Rachold et al., 2004; Fahl and Nöthig, 2007; Semiletov, 1999). Marine

490    organic carbon is derived from open-water production during the ice-free months, export of

491    ice algae, and new production in polynyas (Sakshaug et al., 2004; Nitishinsky et al. 2007).

492    Generally, marine productivity in the Laptev Sea is low and controlled by the nutrients

493    derived from Atlantic water, but spring outflow from the Lena River provides an additional

494    temporary land-derived nutrient source (Pivovarov et al., 1999; Sakshaug et al., 2004;

495    Nitishinsky et al., 2007; Bourgeois et al., 2017) during late spring ice melt (Raymond et al.,

496    2007). Terrestrial-derived nutrients can also affect marine productivity directly by new

497    production, or indirectly, due to plankton production from remineralized, terrestrial-derived

498    dissolved organic carbon and particulate organic carbon (Alling et al., 2012; Tesi et al., 2017).

499    In the eastern East Siberian and Chukchi Sea, the inflow of nutrient-rich Pacific water

500    supports higher marine primary productivity (e.g., Grebmeier et al., 2006). Ice-rafted transport

501    and bottom boundary layer transport are the two most important modes of particle transport

502    (Wegner et al., 2005; Bauch et al., 2009). Since all sediments sampled in this study were fine-

503    grained siltey clays and clayey silts, coarse-grained woody, ice-rafted material plays only a

504    minor role for deposition of organic matter on the outer shelf and slope sediment. The

505  transport direction of inner shelf sediments may follow the predominant atmospheric regime,

506  which is thought to be linked to the Arctic Oscillation (AO) (Weingartner et al., 1999; Guay

507  et al., 2001; Dimitrenko et al., 2008). During positive AO southwesterly winds lead to

508  generally eastward transport and repeated inshore transport in the benthic boundary layer,

509  whereas negative AO favors southerly winds and a predominantly northward transport (Guay

510  et al., 2001; Dmitrenko et al., 2008). Offshore transport of dissolved and particulate organic

511  matter from the Lean delta to the north can occur with the Transpolar Drift, but terrestrial

512  organic material is also transported eastward and obliquely offshore with the Siberian coastal

513  current receiving additional organic material from the Indigirka and Kolyma rivers (Dudarev

514  et al., 2006; Guo et al., 2007). East of 140ºE, the influence of Pacific-derived nutrient-rich

515  water supporting marine production is stronger the further east and offshore the sampling

516  stations are located (Semiletov et al., 2005) (Fig. 1).

517        Carbon degradation rates in the sediment across the whole Siberian shelf and slope

518  reflect this temporally and spatially diverse distribution of nutrient availability, ice cover,

519  sediment deposition, and current flow regime (Rachold et al., 2004; Dudarev et al., 2006;

520  Semiletov et al., 2005; Sakshaug et al., 2004; Dmitrenko et al., 2005). The proportion of

521  degradable marine-derived organic material at the eastern Stations 50 to 63 on the East

522  Siberian shelf is higher than at the western stations in the Laptev Sea, in line with higher

523  nutrient availability due to the Pacific influence. Ice-free conditions and the opening of water

524  due to northward migration of ice shortly before the sampling likely supported new algal

525  primary production at the shelf stations closest to land leading to enhanced export and

526  deposition on the seafloor. During the time of sampling, only Stations 6 to 27 were ice-free,

527  while Stations 23 and 24 had the longest ice-free condition before sampling. By contrast,

528  Stations 30 to 63 were covered by ice during sampling. New export of reactive organic

529  material explains why $O_2$ uptake rates were the highest at stations 23 and 24 along the shelf to

530  slope transect from station 1 to station 24 (Boetius and Damm, 1998). The same pattern as for

531  the $O_2$ uptake rates is also observed for the sulfate reduction rates indicating that reactive

532  organic matter is also buried below the oxygen penetration depth and mixed sediment layer

533  into the sulfate-reducing zone. This indicates that a greater portion of reactive organic

534  material is buried closer to the Lena delta.

535  Derivation of the carbon isotope composition of the remineralized organic matter using

536  Keeling plots (Fig. 5 b) yielded $\delta^{13}C$ values of remineralized DIC between -18.8 ‰ ± 1.1 ‰

537  (Station 53) and -35.8‰ ± 3.0 ‰ in the lower sediment section of Station 1. In the top 20 cm

538      of sediment at Station 1, the regression yielded an isotope composition of -22.7 ‰ for

539      remineralized DIC. This latter isotopic composition reflects the bulk organic matter

540      composition of sedimentary organic carbon at Station 1, which is -22.3 ‰ (Table 2; Salvado

541      et al (2016). The more depleted values below 20 cm depth suggest that an isotopically distinct

542      fraction of organic matter fuels carbon degradation in the buried sediments. Salvado et al

543      (2016) report terrestrial-derived lignin from sediment at this station pointing to the presence

544      of terrestrial organic matter. Terrestrially derived n-alkanes can have such low $\delta^{13}C$ values

545      (Pagani et al., 2006). Slow degradation of terrestrially derived lipids in these sediments

546      suggests a contribution of terrestrial organic matter to carbon mineralization in slope

547      sediment, in line with the very high $DIC/NH_4^+$ ratio of the porewaters. The contribution of

548      degradable terrestrial organic matter to DIC in slope sediments is also supported by the

549      observation of terrestrially derived biomarkers in porewater DOC of central Arctic Ocean

550      sediment analyzed by FT-ICRMS (Rossel et al., 2016) and deep-water sediment trap data in

551      the central Arctic Ocean (Fahl and Nöthig, 2007), but requires further investigation. Our

552      isotope mass balance calculations indicate that in the Laptev Sea on average 47 % of the

553      remineralized DIC is derived from terrestrial organic carbon. This proportion decreases to an

554      average value of 32% in the East Siberian Sea, in line with a greater marine production in this

555      area due to the inflow of Pacific water (Semiletov et al., 2005, Dudarev et al., 2006; Naidu et

556      al., 2000).

557          Published organic carbon budgets for the Arctic shelves infer an average burial

558      efficiency of about 1% of exported marine OC (Stein and Macdonald, 2004), while terrestrial

559      organic carbon, accounting for about 10% of the organic carbon delivered to the Arctic Ocean

560      bottom, has been suggested to be preserved with about 90% efficiency (Macdonald et al.,

561      2015). In contrast, Semiletov et al. (2016) compiled a large dataset indicating substantial

562      aragonite undersaturation of Arctic shelf bottom waters from the Laptev, the East Siberian,

563      and the Russian part of the Chukchi Sea and inferred widespread remineralization of

564      terrestrial organic matter in the bottom waters and sediments. The observation of strongest

565      aragonite undersaturation in the bottom waters supports a sediment-derived $CO_2$ source or a

566      stagnant bottom boundary layer (Semiletov et al., 2013). It is therefore possible that oxic

567      carbon mineralization in the topmost mm of sediment is a major $CO_2$ source for the overlying

568      water.

569          Since ^{35}S-sulfate reduction rates comprise most of the anaerobic carbon mineralization

570      of sediment buried below the oxygen penetration depth, our assessment includes, in contrast

571 to earlier studies, an assessment of terrestrial organic matter mineralization rates beyond the

572 short time period of oxygen exposure in the topmost mm of sediment. Using shelf

573 sedimentation rates of 0.8 mm $y^{-1}$ for the outer Laptev Sea (Strobl et al., 1988) and 1.4 mm $y^{-1}$

574 for the outer East Siberian Sea (Bröder et al., 2016b), the recovered shelf sediments record a

575 time interval of 250 to 700 years since burial with oxygen exposure times between 2 and 45

576 years. The mineralization rates of the terrestrial and marine carbon fractions were derived

577 from the product of the mass fractions and the depth-integrated anaerobic carbon

578 mineralization rates (Table 4). This approach is only applicable for depth-integrated anaerobic

579 carbon mineralization rates, but not for oxic carbon mineralization, because the depth of

580 oxygen penetration and the DIC measurements cover different depth intervals. The

581 proportions calculated based on the $\delta^{13}C$ composition of DIC deeper in the sediment do not

582 necessarily apply to the topmost mm of sediment. It is therefore not possible to relate the

583 relative fractions of mineralized terrestrial and marine organic matter to discrete depth

584 intervals in the oxic zone.

585 The gradient in carbon mineralization rates measured between Stations 1 and 24 reflect

586 the influence of gradual offshore transport of terrestrial organic material (Bröder et al., 2016a)

587 (Fig. 8A, B). Oxygen uptake rates reported by Boetius and Damm (1998) measured in the

588 early fall of 1993 ranged between 0.16 and 1.56 mmol $m^{-2}$ $d^{-1}$. The rates in our 2014 study

589 (0.81 to 11.49 mmol $m^{-2}$ $d^{-1}$) cover the same water depth range and are significantly higher

590 than those measured in 1993 by Boetius and Damm (1998) using a similar methodology

591 (Student's t-Test <0.01). To some extent, the different rates may reflect seasonal differences,

592 because Boetius and Damm (1998) acquired their data later in the fall. However, the increase

593 may also point to higher organic carbon mass accumulation rates compared to 20 years ago,

594 consistent with a decrease in the annual ice cover over the past 20 years in the Arctic (Arrigo

595 and van Dijken, 2011; Stroeve et al., 2012; Walsh et al., 2017). The data cannot answer

596 whether the higher rates reflect an increase in marine and/or terrestrial accumulation.

597 Fig. 9A compares the oxygen uptake rate of the stations of this study with average

598 oxygen uptake rates from the literature for different shelf, slope, and abyssal plain

599 environments worldwide (Canfield et al., 2005). There is no significant difference in the

600 oxygen consumption rates between the Siberian shelf and slope and other continental margin

601 environments (Student's T-test >0.5). $^{35}S$-sulfate reduction rates in these East Siberian slope

602 sediments are also comparable to those in other slope environments (Fig. 9B), except for the

603 shelf where reduction rates are up to a factor 15 lower. The apparent similarity in sulfate

604    reduction rates for the outer shelf and continental slope sediments of the Siberian Arctic

605    suggests similar reactivity of the organic matter. This is surprising since accumulation rates

606    on the continental slope are probably lower than on the shelf. Accumulation of the organic

607    material on the slope may therefore be related to rapid downslope transport of organic

608    material or rapid offshore transport, e.g., due to transport with ice or as bottom nepheloid

609    layers cascading from the shelf edge (Ivanov and Golovin, 2007).

610

### 611    4.3. Assessment of carbon burial efficiency

612    Reported $^{210}$Pb-based sediment accumulation rates in outer Siberian shelf sediment

613    range between 0.05±0.02 g cm$^{-2}$ y$^{-1}$ in the Laptev Sea (Strobl et al., 1988) and 0.24±0.04 g

614    cm$^{-2}$ y$^{-1}$ in the East Siberian Sea (Bröder et al., 2016b). Given surface sediment organic

615    carbon concentrations for this area between 1% and 1.5%, the resulting organic carbon mass

616    accumulation rates vary between 1.1 mmol m$^{-2}$ d$^{-1}$ and 1.7 mmol m$^{-2}$ d$^{-1}$ for the Laptev Sea

617    (area near Station 23), and between 5.5 and 8.2 mmol m$^{-2}$ d$^{-1}$ in the East Siberian Sea (data for

618    Station 63). A comparison with the total oxygen uptake indicates that the $^{210}$Pb-based $C_{org}$

619    accumulation rates on the shelf are equal or significantly lower than the oxygen uptake rates,

620    with a discrepancy of up to a factor 10. Since the $^{210}$Pb data cover the same depth range as our

621    direct degradation rate measurements, $C_{org}$ mass accumulation rates and anaerobic

622    degradation rate measurements cover the same time window of sediment burial. Temporal

623    variation in sediment accumulation therefore cannot explain the discrepancy. The best

624    explanation is that the $^{210}$Pb mass accumulation rates underestimate the true $C_{org}$ mass

625    accumulation rate. Labile organic carbon is oxidized at the sediment surface and is not

626    adequately accounted for in the $C_{org}$ measurements, likely due to coarse sediment sampling

627    resolution. A better account of the true mass accumulation of organic carbon is therefore the

628    sum of the oxygen uptake converted to $CO_2$ equivalents plus the $^{210}$Pb-based $C_{org}$ mass

629    accumulation.

630    We estimated the total burial efficiency of organic carbon from the sum of the depth-

631    integrated aerobic and anaerobic degradation relative to the sum of the $CO_2$ equivalent from

632    $O_2$ uptake and the $^{210}$Pb mass accumulation rate of organic carbon. The resulting burial

633    efficiency of the total organic carbon is on average 28 ± 10 % in the Laptev Sea and 52 ± 11

634    % for the East Siberian Sea. Based on the measured oxygen uptake rates this freshly deposited

635    organic material has substantially higher degradation rates within the top mm of sediment as

636  reflected by the steep $O_2$ gradients. It is likely that this labile fraction consists of more marine

637  than terrestrial organic matter, but the degradation kinetics of these two pools in the oxic zone

638  cannot be assessed reliably with these measurements.

639

640  **4.4. Regional estimates**

641      We present areal estimates of sediment carbon mineralization by extrapolating the

642  measured carbon mineralization rates over the outer Laptev Sea and East Siberian Sea shelf.

643  Such extrapolations of benthic carbon mineralization rates are notoriously difficult given

644  sediment heterogeneity and insufficient temporal data coverage of benthic carbon

645  mineralization rates. For this investigation, no near-shore or slope stations were included in

646  the assessment. The near-shore Siberian shelf environments are under much stronger

647  influence by coastal erosion and riverine discharge than the outer shelf stations and have

648  considerable longer open-water conditions than the outer shelf stations investigated here. In

649  addition, the sedimentation pattern in the near-shore environments is significantly more

650  diverse, which will affect sedimentation rates, grain size distribution, and carbon contents. For

651  this reason, we did not extend our extrapolations to the inner shelf environments. Some of

652  these inner shelf settings likely have much higher benthic carbon mineralization rates and

653  additional studies are required to constrain these better. Our coverage of the slope stations is

654  insufficient for meaningful spatial extrapolations.

655      We estimate the extent of the outer shelf area with depositional conditions comparable

656  to those investigated here to cover approximately 280,000 km$^2$ of the Laptev Sea. For the East

657  Siberian Sea, we estimate the respective area of the outer shelf to be 340,000 km$^2$. Due to the

658  stronger terrestrial influence in the Laptev Sea, we calculated rates separately for the two shelf

659  seas. The areal coverage with sediment stations was too sparse for statistically significant

660  interpolations between stations to give reliable spatial accounts of the gradients in rates

661  between the stations. Instead, arithmetic averages of sediment mineralization rates and fluxes

662  were calculated for these regions. Accepting the uncertainties in our assessment, we estimate

663  that the calculated areal rates could deviate by up to 50%. Table 5 lists the calculated rates

664  based on the average flux calculated per square meter per day for oxygen uptake, DIC flux,

665  bacterial sulfate reduction, and total anaerobic carbon mineralization. Our $O_2$ uptake

666  calculations suggest that 5.2 and 10.4 Tg C y$^{-1}$ are released from outer shelf sediment in the

667  Laptev and East Siberian Sea, respectively, totaling 15.9 Tg C y$^{-1}$ for the whole investigated

668    area (Table 5). The rates calculated with our data set agree well with the $O_2$ uptake rates

669    recently published by Bourgeois et al. (2017) for the Laptev Sea. Anaerobic carbon

670    mineralization based on DIC, ^{35}S-SRR and combined manganese, iron, and sulfate reduction

671    range between 0.62 and 1.28 Tg C $y^{-1}$. Between 0.25 and 0.48 Tg C $y^{-1}$ are attributed to the

672    anaerobic oxidation of terrestrially derived organic material, which represents 0.5 % to 8 % of

673    the annual terrestrial organic matter load to the Laptev and East Siberian Sea ranging from 6

674    Tg $y^{-1}$ (Stein and Macdonald, 2004) to 22 ± 8 Tg $y^{-1}$ (Vonk et al., 2012). The anaerobic

675    degradation is thus five to ten times lower than the estimated annual water column

676    degradation of particulate terrestrial organic matter in the Eastern Siberian Arctic shelf system

677    of 2.5 ± 1.6 Tg C $y^{-1}$ (Sanchez et al. 2011), and represents between 0.5% and 2% of the

678    annual organic carbon export from land.

679    There are large uncertainties associated with these estimates, given that our

680    calculations do not account for carbon mineralization of resuspended terrestrial organic

681    material and likely higher rates of mineralization in inner shelf sediments. Nevertheless, these

682    data indicate that the contribution of the benthic DIC flux to the total $CO_2$ production in the

683    outer Eastern Siberian Sea and Laptev Sea is small. This conclusion, however, does not

684    necessarily extend to the inner parts of the Laptev Sea and the western parts of the East

685    Siberian Sea, where $CO_2$ supersaturation has been reported by Semiletov et al. (2012) and

686    Pipko et al. (2011). Anderson et al (2009) estimated a DIC excess of 10 Tg C by evaluating

687    data from the Laptev and East Siberian Seas collected in the summer of 2008 and suggested

688    that this excess was caused mainly by terrestrial organic matter decomposition. Their estimate

689    can be compared to our sediment oxygen uptake for the outer Laptev and East Siberian Sea

690    shelf of almost 16 Tg $O_2$ $y^{-1}$, which would demand that 62.5 % of the oxygen uptake was due

691    to terrestrial organic matter mineralization. However, the reported annual production of

692    marine organic matter for the total Laptev and East Siberian Sea is about 46 Tg C $y^{-1}$ (Stein

693    and Macdonald, 2004). Even if only half of this amount is produced in the outer shelf region

694    and another half of that amount is deposited on the sea floor, there would still be more than 10

695    Tg C $y^{-1}$ of reactive marine organic matter available at the sediment surface. Our data would

696    therefore suggest that at least in the more productive East Siberian Sea the pronounced

697    aragonite undersaturation reported for bottom waters in the East Siberian Sea is probably to

698    aerobic mineralization of largely marine organic matter with a lesser contribution from

699    terrestrial organic matter.

700

## 5. Conclusions

In Laptev and East Siberian Sea shelf and slope sediment between 47 and 32% of the DIC in porewaters is derived from terrestrial organic matter mineralization, which occurs largely by bacterial sulfate reduction. This conclusion confirms previous observations that terrestrial organic carbon buried in Siberian shelf and slope sediment is not conservative (Semiletov et al., 2013; Karlsson et al., 2015; Bröder et al., 2016b). While mineralization of terrestrial organic material has been reported for the shelf waters and resuspended surface sediment, our data extend this observation to anaerobic degradation in buried sediment. When compared to estimates of the terrestrial organic carbon load to the shelf, terrestrial carbon mineralization in buried sediment under anaerobic conditions is minor. Mass balance considerations suggest that the greater part of the oxygen consumption in the top cm of sediment is due to marine organic matter mineralization and that the degrading marine proportion in the oxic zone is higher than in the anaerobic zone. Further studies are required to better quantify the contribution of terrestrial carbon mineralization under aerobic conditions. Future changes in terrestrial organic carbon load and marine production on the Siberian shelf under longer ice-free conditions (Arrigo and van Dijken, 2011) on the East Siberian shelf will likely change the present-day proportions of degrading marine and terrestrial organic matter further. This requires continued long-term studies of carbon mineralization at the seafloor to assess the effect of sediment carbon mineralization for the $CO_2$ inventory of this shallow shelf sea.

## 6. Acknowledgements

Funding for this investigation came from the K&A Wallenberg foundation, the Swedish Polarsekretariat, and the Bolin Centre for Climate Research at Stockholm University. Igor Semiletov acknowledge support from the Russian Government (No. 14.Z50.31.0012/03.19.2014). We would like to thank the members of the SWERUS-C3 consortium, the shipcrew on icebreaker Oden, and Heike Siegmund, Lina Hansson, Barkas Charalampos, and Dimitra Panagiotopoulou for help with the laboratory work. We dedicate this publication to our friend and colleague Vladimir Samarkin, who unfortunately passed away before publication of this work. This manuscript benefitted from discussions with Patrick Crill, Rienk Smittenberg, Örjan Gustafsson, Christoph Humborg, Julia Steinbach,

732 Clint Miller, Marc Geibel, Emma Karlsson, Brett Thornton, Jorien Vonk, Leif Anderson, and

733 Magnus Mörth.

734

735 **7. References**

736

737 Alling, V., Sanchez-Garcia, L., Porcelli, D., Pugach, S., Vonk, J. E., van Dongen, B., Mörth,

738 C.-M., Anderson, L. G.,  Sokolov, A., Andersson, P., Humborg, C., Semiletov, I., and

739 Gustafsson, Ö.: Non-conservative behavior of dissolved organic carbon across the Laptev and

740 East Siberian seas, Global Biogeochemical Cycles, 24, 10.1029/2010gb003834, 2010.

741 Alling, V., Porcelli, D., Mörth, C. M., Anderson, L. G., Sanchez-Garcia, L., Gustafsson, Ö.,

742 Andersson, P. S., and Humborg, C.: Degradation of terrestrial organic carbon, primary

743 production and out-gassing of $CO_2$ in the Laptev and East Siberian Seas as inferred from $\delta^{13}C$

744 values of DIC, Geochimica et Cosmochimica Acta, 95, 143-159, 2012.

745 Anderson LG, Jutterström S, Hjalmarsson S, Wahlstrom I, Semiletov IP.  Out-gassing of $CO_2$

746 from Siberian Shelf seas by terrestrial organic matter decomposition. Geophysical Research

747 Letters, **36**, L20601, 2009.

748 Arrigo, K. R., and van Dijken, G. L.: Secular trends in Arctic Ocean net primary production,

749 Journal of Geophysical Research: Oceans, 116, 10.1029/2011JC007151, 2011.

750 Bauch, D., Dmitrenko, I., Kirillov, S., Wegner, C., Hölemann, J., Pivovarov, S., Timokhov,

751 L., and Kassens, H.: Eurasian Arctic shelf hydrography: Exchange and residence time of

752 southern Laptev Sea waters, Continental Shelf Research, 29, 1815-1820, 2009.

753 Berg, P., Petersen-Risgaard, N., and Rysgaard, S.: Interpretation and measured concentration

754 profiles in sediment pore water, Limnology and Oceanography, 43, 1500-1510, 1998.

755 Berg, P., Rysgaard, S., and Thamdrup, B.: Dynamic modeling of early diagenesis and nutrient

756 cycling. A case study in an Arctic marine sediment, Amer. J. Sci, 303, 906-955, 2003.

757 Boetius, A., and Damm, E.: Benthic oxygen uptake, hydrolytic potentials and microbial

758 biomass at the Arctic continental slope, Deep Sea Research Part I: Oceanographic Research

759 Papers, 45, 239-275, 1998.

760      Boudreau, B. P.: Diagenetic models and their implementation, Springer Verlag, 414 pp.,

761      1996.

762      Bourgeois, S., Archambault, P., and Witte, U.: Organic matter remineralization in marine

763      sediments: A Pan-Arctic synthesis, Global Biogeochemical Cycles, 31, 190-213, 2017.

764      Bröder, L.-M., Tesi, T., Salvado, J. A., Semiletov, I., Dudarev, O. V., and Gustafsson, Ö.:

765      Fate of terrigeneous organic matter across the Laptev Sea from the mouth of the Lena River to

766      the deep sea of the Arctic interior, Biogeosciences, 13, 5003-5019, 2016a.

767      Bröder, L., Tesi, T., Andersson, A., Eglinton, T. I., Semiletov, I. P., Dudarev, O. V., Roos, P.,

768      and Gustafsson, Ö.: Historical records of organic matter supply and degradation status in the

769      East Siberian Sea, Organic Geochemistry, 91, 16-30, 2016b.

770      Canfield, D. E., Kristensen, E., and Thamdrup, B.: Aquatic geomicrobiology, Advances in

771      marine biology, 48, 2005.

772      Dmitrenko, I. A., Tyshko, K. N., Kirillov, S. A., Eicken, H., Hölemann, J. A., and Kassens,

773      H.: Impact of flaw polynyas on the hydrography of the Laptev Sea, Global and Planetary

774      Change, 48, 9-27, 2005.

775      Dmitrenko, I. A., Kirillov, S. A., and Tremblay, L. B.: The long                             -term and interannual

776      variability of summer fresh water storage over the eastern Siberian shelf: Implication for

777      climatic change, Journal of Geophysical Research: Oceans, 113, doi: 10.1029/2007JC004304,

778      2008.

779      Dudarev, O. V., Semiletov, I. P., and Charkin, A. N.: Particulate material composition in the

780      Lena River-Laptev Sea system: Scales of heterogeneities. In: Doklady Earth Sciences, 6,

781      1000-1005, 2006.

782      Fahl, K., and Nöthig, E.-M.: Lithogenic and biogenic particle fluxes on the Lomonosov Ridge

783      (central Arctic Ocean) and their relevance for sediment accumulation: Vertical vs. lateral

784      transport, Deep Sea Research Part I: Oceanographic Research Papers, 54, 1256-1272, 2007.

785      Glud, R. N.: Oxygen dynamics of marine sediments, Mar. Biol. Res., 4, 243-289, 2008.

786      Grebmeier, J. M., Cooper, L. W., Feder, H. M., and Sirenko, B. I.: Ecosystem dynamics of the

787      Pacific-influenced Northern Bering and Chukchi Seas in the Amerasian Arctic, Progress in

788      Oceanography, 71, 331-361, 2006.

789    Guay, C. K., Falkner, K. K., Muench, R. D., Mensch, M., Frank, M., and Bayer, R.: Wind  -

790    driven transport pathways for Eurasian Arctic river discharge, Journal of Geophysical

791    Research: Oceans, 106, 11469-11480, 2001.

792    Guo, L., Ping, C. L., and Macdonald, R. W.: Mobilization pathways of organic carbon from

793    permafrost to arctic rivers in a changing climate, Geophysical Research Letters, 34, 2007.

794    Hall, P. O. J., and Aller, R. C.: Rapid, small-volume flow injection analysis for $\Sigma CO_2$ and

795    $NH_4^+$ in marine and freshwaters, Limnology and Oceanography, 37, 1113-1119, 1992.

796    Hugelius, G., Strauss, J., Zubrzycki, S., Harden, J. W., Schuur, E. A. G., Ping, C. L.,

797    Schirrmeister, L., Grosse, G., Michaelson, G. J., Koven, C. D., O'Donnell, J. A., Elberling, B.,

798    Mishra, U., Camill, P., Yu, Z., Palmtag, J., and Kuhry, P.: Estimated stocks of circumpolar

799    permafrost carbon with quantified uncertainty ranges and identified data gaps,

800    Biogeosciences, 11, 6573-6593, 2014.

801    Ivanov, V. V. and Golovin, P. N.: Observations and modeling of dense water cascading from

802    the northwestern Laptev Sea shelf, Journal of Geophysical Research: Oceans, 112, 2007.

803    Jørgensen, B. B.: A comparison of methods for the quantification of bacterial sulfate

804    reduction in coastal marine sediments: I. Measurement with radiotracer techniques,

805    Geomicrobiology Journal, 1, 11-27, 1978.

806    Jørgensen, B. B., and Kasten, S.: Sulfur and methane oxidation, in: Marine Geochemistry,

807    Second Edition ed., edited by: Schulz, H. D., and Zabel, M., Springer Verlag, Berlin

808    Heidelberg, 271-309, 2006.

809    Kallmeyer, J., Ferdelman, T. G., Weber, A., Fossing, H., and Jørgensen, B. B.: Evaluation of

810    a cold chromium distillation procedure for recovering very small amounts of radiolabeled

811    sulfide related to sulfate reduction measurements., Limnol. Oceanog. Methods, 2, 171-180,

812    2004.

813    Karlsson, E. S., Brüchert, V., Tesi, T., Charkin, A., Dudarev, O., Semiletov, I., and

814    Gustafsson, Ö.: Contrasting regimes for organic matter degradation in the East Siberian Sea

815    and the Laptev Sea assessed through microbial incubations and molecular markers, Marine

816    Chemistry, 170, 11-22, 2015.

817    Koven, C. D., Lawrence, D. M., and Riley, W. J.: Permafrost carbon-climate feedback is

818    sensitive to deep soil carbon decomposability but not deep soil nitrogen dynamics,

819    Proceedings of the National Academies of Science, 112, 3752-3757, 2015.

820    Lalonde, K., Mucci, A., Ouellet, A., and Gelinas, Y.: Preservation of organic matter in

821    sediments promoted by iron, Nature, 483, 198-200, 2012.

822    Li, Y.-H. and Gregory, S.: Diffusion of ions in sea water and in deep-sea sediments,

823    Geochimica et Cosmochimica Acta, 88, 703-714, 1974.

824    Macdonald, R. W., and Gobeil, C.: Manganese Sources and Sinks in the Arctic Ocean with

825    Reference to Periodic Enrichments in Basin Sediments, Aquatic Geochemistry, 18, 565-591,

826    2012.

827    Mackin, J. E., and Aller, R.C.: Ammonium adsorption in marine sediments, Limnology and

828    Oceanography, 29, 250-257, 1984.

829    Macdonald, R. W., Kuzyk, Z. Z. A., and Johannessen, S. C.: The vulnerability of Arctic shelf

830    sediments to climate change, Environmental Reviews, 1-19, 2015.

831    McGuire, A. D., Anderson, L. G., Christensen, T. R., Dallimore, S., Guo, L., Hayes, D. J.,

832    Heimann, M., Lorenson, T. D., Macdonald, R. W., and Roulet, N.: Sensitivity of the carbon

833    cycle in the Arctic to climate change, Ecological Monographs, 79, 523-555, 2009.

834    McTigue, N., Gardner, W., Dunton, K., and Hardison, A.: Biotic and abiotic controls on co-

835    occurring nitrogen cycling processes in shallow Arctic shelf sediments, Nature

836    Communications, 7, 2016.

837    Miller, C. M., Dickens, G. R., Jakobsson, M., Johansson, C., Koshurnikov, A., O'Regan, M.,

838    Muschitiello, F., Stranne, C., and Mörth, C.-M.: Low methane concentrations in sediment

839    along the continental slope north of Siberia: Inference from pore water geochemistry,

840    Biogeosciences Discussions, doi:10.5194/bg-2016-308, 2016.

841    Naidu, A. S., Cooper, L. W., Finney, B. P., Macdonald, R. W., Alexander, C., and Semiletov,

842    I. P.: Organic carbon isotope ratios ($\delta^{13}$C) of Arctic Amerasian Continental shelf sediments.

843    International Journal of Earth Sciences, 89, 522-532, 2000.

844    Nickel, M., Vandieken, V., Brüchert, V., and Jørgensen, B. B.: Microbial Mn(IV) and Fe(III)

845    reduction in northern Barents Sea sediments under different conditions of ice cover and

846    organic carbon deposition, Deep Sea Research Part II: Topical Studies in Oceanography, 55,

847    2390-2398, 2008.

848    Nitishinsky, M., Anderson, L. G., and Hölemann, J. A.: Inorganic carbon and nutrient fluxes

849    on the Arctic Shelf, Continental Shelf Research, 27, 1584-1599, 2007.

850    Pipko, I., Semiletov I.P., Pugach S.P., Wahlstrom I., Anderson L.G. Interannual variability of

851    air-sea $CO_2$ fluxes and carbon system in the East Siberian Sea. Biogeosciences, **8**, 1987-2007,

852    2011.

853    Pivovarov, S., Hölemann, J., Kassens, H., Antonow, M., and Dmitrenko, I.: Dissolved

854    oxygen,silicon,phosphorous and suspended matter concentrations during the spring breakup

855    of the Lena River, in: Land–Ocean Systems in the Siberian Arctic:Dynamics and History,

856    edited by: Kassens, H., Bauch, H. A., Dmitrenko, I., Eicken, H., Hubberten, H.-W., Melles,

857    M., Thiede, J., and Timokhov, L., Springer, Berlin, 251-264, 1999.

858    Qi, D., Chen, L., Chen, B., Gao, Z., Zhong, W., Feely, R. A., Anderson, L. G., Sun, H., Chen,

859    J., Chen, M., Zhan, L., Zhang, Y., and Cai, W.-J.: Increase in acidifying water in the western

860    Arctic Ocean, Nature Clim. Change, 7, 195-199, 2017.

861    Rachold, V., Eicken, H., Gordeev, V., Grigoriev, M. N., Hubberten, H.-W., Lisitzin, A. P.,

862    Shevchenko, V., and Schirrmeister, L.: Modern terrigenous organic carbon input to the Arctic

863    Ocean, in: The organic carbon cycle in the Arctic Ocean, Springer, 33-55, 2004.

864    Rasmussen, H., and Jørgensen, B. B.: Microelectrode studies of seasonal oxygen uptake in a

865    coastal sediment: Role of molecular diffusion, Marine ecology progress series. Oldendorf, 81,

866    289-303, 1992.

867    Raymond, P. A., McClelland, J., Holmes, R., Zhulidov, A., Mull, K., Peterson, B., Striegl, R.,

868    Aiken, G., and Gurtovaya, T.: Flux and age of dissolved organic carbon exported to the Arctic

869    Ocean: A carbon isotopic study of the five largest arctic rivers, Global Biogeochemical

870    Cycles, 21, 10.1029/2007GB002983, 2007.

871    Rekant, P., Bauch, H. A., Schwenk, T., Portnov, A., Gusev, E., Spiess, V., Cherkashov, G.,

872    and Kassens, H.: Evolution of subsea permafrost landscapes in Arctic Siberia since the Late

873    Pleistocene: a synoptic insight from acoustic data of the Laptev Sea, Arktos, 1,

874    10.1007/s41063-015-0011-y, 2015.

875 Rossel, P. E., Bienhold, C., Boetius, A., and Dittmar, T.: Dissolved organic matter in pore
876 water of Arctic Ocean sediments: Environmental influence on molecular composition,
877 Organic Geochemistry, 97, 41-52, 2016.

878 Sakshaug, E.: Primary and secondary production in the Arctic Seas, in: The organic carbon
879 cycle in the Arctic Ocean, Springer, 57-81, 2004.

880 Salvadó, J. A., Tesi, T., Andersson, A., Ingri, J., Dudarev, O. V., Semiletov, I. P., and
881 Gustafsson, Ö.: Organic carbon remobilized from thawing permafrost is resequestered by
882 reactive iron on the Eurasian Arctic Shelf, Geophysical Research Letters, 42, 8122-8130,
883 2015.

884 Sánchez-García, L., Alling, V., Pugach, S., Vonk, J., van Dongen, B., Humborg, C., Dudarev,
885 O., Semiletov, I., and Gustafsson, Ö.: Inventories and behavior of particulate organic carbon
886 in the Laptev and East Siberian seas, Global Biogeochemical Cycles, 25,
887 10.1029/2010gb003862, 2011.

888 Savvichev, A., Rusanov, I., Pimenov, N., Zakharova, E., Veslopolova, E., Lein, A. Y., Crane,
889 K., and Ivanov, M.: Microbial processes of the carbon and sulfur cycles in the Chukchi Sea,
890 Microbiology, 76, 603-613, 2007.

891 Schuur, E. A. G., McGuire, A. D., Schadel, C., Grosse, G., Harden, J. W., Hayes, D. J.,
892 Hugelius, G., Koven, C. D., Kuhry, P., Lawrence, D. M., Natali, S. M., Olefeldt, D.,
893 Romanovsky, V. E., Schaefer, K., Turetsky, M. R., Treat, C. C., and Vonk, J. E.: Climate
894 change and the permafrost carbon feedback, Nature, 520, 171-179, 2015.

895 Seeberg-Elverfeldt, J., Schlüter, M., Feseker, T., and Kölling, M.: Rhizon sampling of
896 porewaters near the sediment-water interface of aquatic systems, Limnol. Oceanogr. Methods,
897 3, 361-371, 2005.

898 Semiletov, I., Dudarev, O., Luchin, V., Charkin, A., Shin, K.-H., and Tanaka, N.: The East
899 Siberian Sea as a transition zone between Pacific-derived waters and Arctic shelf waters,
900 Geophysical Research Letters, 10.1029/2005GL022490, 2005.

901 Semiletov, I., Pipko, I., Gustafsson, Ö., Anderson, L. G., Sergienko, V., Pugach, S., Dudarev,
902 O., Charkin, A., Gukov, A., Broder, L., Andersson, A., Spivak, E., and Shakhova, N.:
903 Acidification of East Siberian Arctic Shelf waters through addition of freshwater and
904 terrestrial carbon, Nature Geoscience, 9, 361-365, 2016.

905 Semiletov I.P., Shakhova, N.E, Pipko, I.I.: Space-time dynamics of carbon and environmental
906 parameters related to carbon dioxide emissions in the Buor-Khaya Bay and adjacent part of
907 the Laptev Sea. Biogeosciences, **10**, 5977-5996, 2013.

908 Semiletov I.P., Pipko I.I., Shakhova N.E., Dudarev O.V., Pugach S.P., Charkin A.N., McRoy
909 C.P., Kosmach D., and Ö. Gustafsson.: Carbon transport by the Lena River from its
910 headwaters to the Arctic Ocean, with emphasis on fluvial input of terrestrial particulate
911 organic carbon vs. carbon transport by coastal erosion. Biogeosciences, **8**, 2407-2426, 2011.

912 Semiletov, I.P., Destruction of the coastal permafrost ground as an important factor in
913 biogeochemistry of the Arctic Shelf waters, Trans. (Doklady) Russian Acad. Sci., 368, 679-
914 682, 1999 (translated into English).

915 Stein, R., and Macdonald, R. W.: The Organic Carbon Cycle in the Arctic Ocean, Springer-
916 Verlag, Berlin, 382 pp., 2004.

917 Strobl, C., Schulz, V., Vogler, S., Baumann, S., Kassens, H., Kubik, P. W., Suter, M., and
918 Mangini, A.: Determination of depositional beryllium-10 fluxes in the area of the Laptev Sea
919 and beryllium-10 concentrations in water samples of high northern latitudes, in: Land-Ocean
920 Systems in the Siberian Arctic: Dynamics and History, edited by: Kassens, H., Bauch, H. A.,
921 Dmitrenko, I., Eicken, H., Hubberten, H.-W., Melles, M., Thiede, J., and Timokhov, L.,
922 Springer, Berlin, 515-532, 1998.

923 Tarnocai, C., Canadell, J. G., Schuur, E. A. G., Kuhry, P., Mazhitova, G., and Zimov, S.: Soil
924 organic carbon pools in the northern circumpolar permafrost region, Global Biogeochemical
925 Cycles, 23, 10.1029/2008gb003327, 2009.

926 Tesi, T., Semiletov, I., Hugelius, G., Dudarev, O., Kuhry, P., and Gustafsson, Ö.:
927 Composition and fate of terrigenous organic matter along the Arctic land–ocean continuum in
928 East Siberia: Insights from biomarkers and carbon isotopes, Geochimica et Cosmochimica
929 Acta, 133, 235-256, 2014.

930 Tesi, T., Semiletov, I., Dudarev, O., Andersson, A., and Gustafsson, Ö.: Matrix association
931 effects on hydrodynamic sorting and degradation of terrestrial organic matter during cross-
932 shelf transport in the Laptev and East Siberian shelf seas, Journal of Geophysical Research:
933 Biogeosciences, 121, 731-752, 2016.

934 Tesi, T., Geibel, M. C., Pearce, C., Panova, E., Vonk, J. E., Karlsson, E., Salvado, J. A.,

935 Kruså, M., Bröder, L., Humborg, C., Semiletov, I., and Gustafsson, Ö.: Carbon geochemistry

936 of plankton-dominated samples in the Laptev and East Siberian shelves: contrasts in

937 suspended particle composition, Ocean Sci., 13, 735-748, 10.5194/os-13-735-2017, 2017.

938 Thamdrup, B.: Bacterial manganese and iron reduction in aquatic sediments, Advances in

939 Microbial Ecology, 16, 41-84, 2000.

940 Arrigo, K. R., and van Dijken, G. L.: Secular trends in Arctic Ocean net primary production,

941 Journal of Geophysical Research: Oceans, 116, 10.1029/2011JC007151, 2011.

942 Hugelius, G., Strauss, J., Zubrzycki, S., Harden, J. W., Schuur, E. A. G., Ping, C. L.,

943 Schirrmeister, L., Grosse, G., Michaelson, G. J., Koven, C. D., O'Donnell, J. A., Elberling, B.,

944 Mishra, U., Camill, P., Yu, Z., Palmtag, J., and Kuhry, P.: Estimated stocks of circumpolar

945 permafrost carbon with quantified uncertainty ranges and identified data gaps,

946 Biogeosciences, 11, 6573-6593, 2014.

947 Qi, D., Chen, L., Chen, B., Gao, Z., Zhong, W., Feely, R. A., Anderson, L. G., Sun, H., Chen,

948 J., Chen, M., Zhan, L., Zhang, Y., and Cai, W.-J.: Increase in acidifying water in the western

949 Arctic Ocean, Nature Clim. Change, 7, 195-199, 2017.

950 Sánchez-García, L., Alling, V., Pugach, S., Vonk, J., van Dongen, B., Humborg, C., Dudarev,

951 O., Semiletov, I., and Gustafsson, Ö.: Inventories and behavior of particulate organic carbon

952 in the Laptev and East Siberian seas, Global Biogeochemical Cycles, 25,

953 10.1029/2010gb003862, 2011.

954 Vandieken, V., Nickel, M., and Jørgensen, B. B.: Carbon mineralization in Arctic sediments

955 northeast of Svalbard: (Mn(IV) and Fe(III) reduction as principal anaerobic respiratory

956 pathways, Marine Ecology Progress Series, 322, 15-27, 2006.

957 Vonk, J. E., Sanchez-Garcia, L., van Dongen, B. E., Alling, V., Kosmach, D., Charkin, A.,

958 Semiletov, I. P., Dudarev, O. V., Shakhova, N., Roos, P., Eglinton, T. I., Andersson, A., and

959 Gustafsson, O.: Activation of old carbon by erosion of coastal and subsea permafrost in Arctic

960 Siberia, Nature, 489, 137-140.

961 Wegner, C., Hölemann, J. A., Dmitrenko, I., Kirillov, S., and Kassens, H.: Seasonal variations

962 in Arctic sediment dynamics—evidence from 1-year records in the Laptev Sea (Siberian

963 Arctic), Global and Planetary Change, 48, 126-140, 2005.

964    Wegner, C., Bauch, D., Hölemann, J. A., Janout, M. A., Heim, B., Novikhin, A., Kassens, H.,

965    and Timokhov, L.: Interannual variability of surface and bottom sediment transport on the

966    Laptev Sea shelf during summer, Biogeosciences, 10, 1117-1129, 2013.

967    Weingartner, T. J., Danielson, S., Sasaki, Y., Pavlov, V., and Kulakov, M.: The Siberian

968    Coastal Current: A wind- and buoyancy-forced Arctic coastal current, Journal of Geophysical

969    Research: Oceans, 104, 29697-29713, 1999.

970

971    **List of Tables**

972

973    Table 1. Physical and chemical characteristics of sediment and bottom water chemical
974    characteristics at the sampled stations.

975    Table 2. $O_2$ uptake, integrated $^{35}$S-sulfate reduction rates, DIC flux, and porewater DIC/$NH_4^+$
976    ratios.

977    Table 3. Anaerobic rates of carbon mineralization by manganese, iron, and sulfate reduction.

978    Table 4. Calculated carbon isotope composition of remineralized DIC and mass fractions of
979    the marine and terrestrial end member and corresponding terrestrial carbon degradation rates
980    based on $^{35}$S-SRR and DIC.

981    Table 5. Regional estimates of sediment carbon mineralization in the outer Laptev and East
982    Siberian shelf sea.

1009    Fig. 8 A. Map of field area and sampling stations showing oxygen uptake rates. For

1010    comparison, oxygen uptake rates reported in Boetius and Damm (1998) are shown as triangles

1011    using the same color code. B: Map of field area and sampling stations with depth-integrated

1012    sulfate reduction rates.

1013

1014    Fig. 9 A. Water depth variation of sediment oxygen uptake. B: Water depth variation of

1015    integrated $^{35}$S-sulfate reduction rates (0-30 cm sediment depth). For reference average rates of

1016    abyssal plain, continental rise, slope, and shelf sediments, deposition and non-depositional,

1017    are shown for reference.

1018

1019

1020

1021

**Table 1. Physical and chemical characteristics of sediment and bottom water at the sampled stations**

| Station | Latitude °N | Longitude °E | Date Month/Day/Year | Water depth m | Ice cover % | Bottom water salinity ‰ | Bottom water temperature °C | Bottom water O$_2$ concentration µmol/L | Bottom water NH$_4^+$ concentration µmol/L | Bottom water DIC above sediment µmol/L | δ$^{13}$C DIC bottom water ‰ vs. VPDB | δ$^{13}$C surface sediment org C (Salvadó et al. 2017) ‰ vs. VPDB | Sediment description |
|---|---|---|---|---|---|---|---|---|---|---|---|---|---|
| 1 | 78.942 | 125.243 | 7/15/2014 | 3146 | 50 – 75 | 34.9 | -0.9 | 271.9 | 1.65 | 2151.5 | -0.5 | -22.3 | clay, brown |
| 2 | 78.581 | 125.607 | 7/16/2014 | 2900 | 25 – 50 | 34.9 | -0.9 | 275.0 | n.a. | n.a. | n.a. | n.a. | clay, brown |
| 3 | 78.238 | 126.150 | 7/16/2014 | 2601 | < 25 | 34.9 | -0.9 | 280.0 | n.a. | n.a. | n.a. | n.a. | clay, brown |
| 4 | 77.855 | 126.664 | 7/16/2014 | 2106 | < 25 | 34.9 | -0.8 | 289.4 | 1.81 | 2164.5 | -1.6 | -22.5 | clay, brown |
| 6 | 77.142 | 127.378 | 7/17/2014 | 89 | 0.0 | 34.6 | -1.8 | 327.0 | 1.30 | 2213.0 | -2.2 | -23.2 | clay, top 3 cm brown, then gray, fauna on top of sediment |
| 23 | 76.171 | 129.333 | 7/22/2014 | 56 | 0.0 | 34.2 | -1.8 | 303.2 | 1.34 | 2246.3 | -3.2 | -25.0 | silty clay, top 4 cm brown, then gray, brittle stars |
| 24 | 75.599 | 129.558 | 7/24/2014 | 46 | 0.0 | 34.0 | -1.7 | 283.8 | 0.89 | 2244.1 | -2.0 | -24.8 | silty clay, top 4 cm brown, then gray |
| 27 | 76.943 | 132.229 | 7/23/2014 | 44 | 0.0 | 34.2 | -1.8 | 332.3 | 0.94 | 2595.0 | -6.5 | -24.2 | silty clay, top 2 cm brown, then gray, fluffy surface layer, brittle stars |
| 30 | 78.181 | 138.354 | 7/24/2014 | 69 | 0.0 | 34.1 | -1.6 | 334.8 | 0.79 | 2178.4 | -3.7 | -23.4 | silty clay, top 4 cm brown, then gray |
| 31 | 79.396 | 135.497 | 7/25/2014 | 3056 | 0.0 | 34.9 | -0.9 | 270.9 | 0.74 | 2161.7 | n.a. | n.a. | clay, brown |
| 35 | 78.600 | 137.061 | 7/26/2014 | 541 | 0.0 | 34.9 | 0.4 | 288.1 | 0.43 | 2183.7 | n.a. | n.a. | clay top 15cm brown, fluffy, inhomogeneous, surface-dwelling fauna |
| 37 | 78.521 | 137.170 | 7/26/2014 | 205 | 0.0 | 34.7 | 0.0 | 295.4 | 0.89 | 2171.1 | n.a. | n.a. | clay, top 5cm brown, then gray |
| 40 | 77.670 | 144.668 | 7/27/2014 | 45 | 0.0 | 31.5 | -1.3 | 190.3 | 0.53 | 2213.7 | -1.6 | -23.7 | silty clay, top 3cm brown, then gray, brittle stars |
| 43 | 76.780 | 147.791 | 7/28/2014 | 42 | 25-50 | 30.1 | -1.2 | 256.4 | 0.61 | 2086.7 | n.a. | n.a. | silty clay to clayey silt, top 2cm brown, then gray, some small surface-dwelling animals |
| 45 | 76.416 | 148.115 | 7/29/2014 | 40 | < 50 | 29.1 | -1.3 | 319.9 | 0.57 | 2576.0 | -2.1 | -24.4 | silty clay to clayey silt, 2cm brown, then gray-black, rather stiff |
| 48 | 76.615 | 153.345 | 7/30/2014 | 49 | > 75 | 30.6 | -1.6 | 315.9 | 0.50 | 2075.1 | -2.2 | -25.8 | silty clay to clayey silt, top 3cm brown, then grayblack |
| 50 | 75.764 | 158.529 | 8/1/2014 | 44 | > 75 | 31.1 | -1.4 | 311.0 | 0.51 | 2068.7 | -2.1 | -24.6 | silty clay to clayey silt, top 2cm brown, then grayblack |
| 53 | 74.957 | 161.088 | 8/2/2014 | 47 | > 75 | 31.0 | -1.6 | 253.3 | 0.16 | 2086.1 | -2.5 | n.a. | silty clay to clayey silt, top 3 cm brown, then 3 cm gray, then grayblack |
| 58 | 74.440 | 166.050 | 8/4/2014 | 54 | > 75 | 31.4 | -1.7 | 254.3 | 0.65 | 2154.9 | -1.5 | -23.8 | silty clay to clayey silt, slightly resuspended, top 2 cm brown, then gray, soft |
| 63 | 74.685 | 172.361 | 8/7/2014 | 67 | > 75 | 32.4 | -1.4 | 186.0 | 0.61 | 2240.8 | -2.2 | -22.7 | silty clay to clayey silt, top 1cm brown, then gray |

**Table 2. O$_2$ uptake, integrated $^{35}$S-sulfate reduction rates, DIC flux, and porewater DIC/NH$_4^+$ ratios**

| Station | Water depth | mean O$_2$ penetration depth | mean O$_2$ depth | O$_2$ uptake (modelled/measured with 2D optode) | $^{35}$S-SRR (0-30 cm) duplicates | DIC flux (modelled in anaerobic zone/measured with whole core incubation) | Average porewater DIC/NH$_4^+$ |
|---------|-------------|------------------------------|------------------|-------------------------------------------------|-----------------------------------|---------------------------------------------------------------------------|-------------------------------|
| | m | mm | µmol/L | mmol m$^{-2}$ d$^{-1}$ | mmol m$^{-2}$ d$^{-1}$ | mmol m$^{-2}$ d$^{-1}$ | |
| 1 | 3146 | > 60 | 217 | 1.48 ± 0.08 | 0.05 / 0.21 | -0.11 | |
| 2 | 2900 | > 60 | 213 | 1.32 ± 0.05 | | | |
| 3 | 2601 | > 60 | 194 | 0.81 ± 0.06 | | | |
| 4 | 2106 | > 60 | 89 | 1.32 ± 0.05 | 0.17 / 0.17 | -0.15 | |
| 6 | 89 | 36 | 0 | 2.61 ± 0.01 | 0.03 / 0.05 | -0.08 | |
| 23 | 56 | 13 | 0 | 5.00 ± 0.09 ; 5.3 ± 0.2 | 0.56 | -0.12; -5.1 ± 0.4 | 13 |
| 24 | 46 | 10 | 0 | 7.95 ± 0.14 | | -0.22 | 10 |
| 27 | 44 | 16 | 0 | 3.75 ± 0.08 | 0.37 / 0.20 | -0.27 | 12 |
| 30 | 69 | 16 | 0 | 2.61 ± 0.11 | 0.06 / 0.03 | -0.12 | 15 |
| 31 | 3056 | > 60 | 194 | 1.78 ± 0.07 | | | |
| 35 | 541 | > 60 | 30 | 2.43 ± 0.32 | | | |
| 37 | 205 | 44 | 0 | 2.51 ± 0.10 | | | |
| **Average Laptev Sea shelf** | | | | **4.20** | **0.19** | **0.2 ; 5.1** | **12** |
| 40 | 45 | 12 | 0 | 4.62 ± 0.08 | 0.33 / 0.24 | -0.19 | 16 |
| 43 | 42 | 13 | 0 | 4.7 ± 0.10 | | | |
| 45 | 40 | 10 | 0 | 4.02 ± 0.10 | 0.23 / 0.19 | -0.37 | 13 |
| 48 | 49 | 5 | 0 | 9.14 ± 0.22 | 0.68 / 0.53 | -0.71 | 10 |
| 50 | 44 | 9 | 0 | 5.65 ± 0.43; 5.2 ± 0.1 | 1.32 / 1.40 | -1.01 ; -5.2 ± 0.2 | 12 |
| 53 | 47 | 10 | 0 | 4.53 ± 0.08 ; 4.7 ± 0.1 | 0.10 / 0.17 | -0.20 | 14 |
| 58 | 54 | 3 | 0 | 11.49 ± 0.52 | 1.01 | -1.27 | 24 |
| 63 | 67 | 4 | 0 | 10.72 ± 0.15 ; 10.8 ± 0.3 | 1.41 | -1.35 ; -10.8 ± 0.6 | 12 |
| **Average East Siberian Sea shelf** | | | | **7.2** | | **0.7 ; 8.0** | **14** |

**Table 3. Anaerobic rates of carbon mineralization by manganese, iron, and sulfate reduction**

| | Net Fe²⁺ production | Net Mn²⁺ production | C-equivalent Fe + Mn reduction | ³⁵S-Sulfate reduction | C-equivalents total anaerobic mineralization | Oxygen uptake | % Fe + Mn reduction of total anaerobic | Percentage anaerobic C mineralization of total | Percentage Fe and Mn mineralization of total |
|---|---|---|---|---|---|---|---|---|---|
| | mmol m⁻¹ d⁻¹ | | | | | | | % | |
| Station 23 | 0.05 | 0.03 | 0.03 | 0.56 | 1.1 | 5.0 | 2.3 | 22.9 | 0.5 |
| Station 30 | 0.02 | 0.04 | 0.03 | 0.05 | 0.1 | 2.6 | 21.9 | 4.4 | 1.0 |
| Station 45 | 0.14 | 0.12 | 0.09 | 0.21 | 0.5 | 4.0 | 18.3 | 12.8 | 2.3 |
| Station 53 | 0.15 | 0.09 | 0.08 | 0.14 | 0.4 | 4.5 | 23.7 | 7.8 | 1.8 |
| Station 63 | - | 0.50 | 0.25 | 1.41 | 3.1 | 10.7 | 8.1 | 26.0 | 2.3 |

**Table 4. Calculated carbon isotope composition of remineralized DIC and mass fractions of the marine and terrestrial endmembers and corresponding terrestrial carbon degradation rates based on $^{35}$S-SRR and DIC flux**

| Station | Average $\delta^{13}C_{DIC}$ remineralized | Marine end member | Terrestrial end member | $^{35}$S-SRR-based terrestrial degradation rate | DIC-based terrestrial degradation rate |
|---|---|---|---|---|---|
| | ‰ vs. VPDB | Mass fraction | | mmol m$^{-2}$ d$^{-1}$ | mmol m$^{-2}$ d$^{-1}$ |
| 1 | -35.8 | 0.0 | 1.0 | 0.13 | 0.11 |
| 4 | -24.7 | 0.73 | 0.27 | 0.05 | 0.04 |
| 6 | -25.1 | 0.65 | 0.35 | 0.01 | 0.03 |
| 23 | -24.5 | 0.78 | 0.22 | 0.12 | 0.03 |
| 24 | -24.7 | 0.73 | 0.27 | | 0.06 |
| 27 | -25.4 | 0.58 | 0.42 | 0.12 | 0.11 |
| 30 | -28.5 | 0.00 | 1.00 | 0.05 | 0.13 |
| **Average Laptev Sea shelf** | **-25.6** | **0.53** | **0.47** | **0.08** | **0.07** |
| 40 | -21.4 | 0.72 | 0.28 | 0.08 | 0.05 |
| 45 | -22.2 | 0.63 | 0.37 | 0.08 | 0.14 |
| 48 | -23.0 | 0.54 | 0.46 | 0.28 | 0.32 |
| 50 | -24.0 | 0.43 | 0.57 | 0.77 | 0.57 |
| 53 | -18.8 | 1.00 | 0.00 | 0.00 | 0.00 |
| 58 | -22.6 | 0.59 | 0.41 | 0.42 | 0.53 |
| 63 | -20.3 | 0.84 | 0.16 | 0.25 | 0.22 |
| **Average East Siberian Sea shelf** | **-21.8** | **0.68** | **0.32** | **0.27** | **0.26** |

**Table 5. Regional estimates of sediment carbon mineralization in the outer Laptev and East Siberian shelf sea**

| | | | Dissolved O$_2$ uptake | Upward DIC flux (anaerobic) | Terrestrial OC-derived DIC flux (anaerobic) | Marine OC-derived DIC flux (anaerobic) | Depth-integrated $^{35}$S-SRR (C equivalent) |
|---|---|---|---|---|---|---|---|
| Outer Laptev Sea | Average | mmol m$^{-2}$ d$^{-1}$ | 4.2 | 0.16 | 0.07 | 0.09 | 0.09 |
| Outer East Siberian Sea | Average | mmol m$^{-2}$ d$^{-1}$ | 7.2 | 0.73 | 0.26 | 0.47 | 0.34 |
| Outer Laptev Sea | 280,000 km$^2$ | Tg C y$^{-1}$ | 5.2 | 0.20 | 0.09 | 0.11 | 0.11 |
| Outer East Siberian Sea | 340,000 km$^2$ | Tg C y$^{-1}$ | 10.8 | 1.09 | 0.39 | 0.70 | 0.50 |
| Total outer shelf area | 620,000 km$^2$ | Tg C y$^{-1}$ | 15.9 | 1.28 | 0.48 | 0.81 | 0.62 |

| | | | $^{35}$S-SRR-based terrestrial C degradation | $^{35}$S-SRR-based marine C degradation | Total TEAP-based anaerobic OC degradation rate | Total TEAP-based anaerobic terrestrial OC degradation rate | Total TEAP-based anaerobic marine OC degradation rate |
|---|---|---|---|---|---|---|---|
| Outer Laptev Sea | Average | mmol m$^{-2}$ d$^{-1}$ | 0.04 | 0.05 | 0.15 | 0.05 | 0.10 |
| Outer East Siberian Sea | Average | mmol m$^{-2}$ d$^{-1}$ | 0.13 | 0.21 | 0.42 | 0.16 | 0.26 |
| Outer Laptev Sea | 280,000 km$^2$ | Tg C y$^{-1}$ | 0.05 | 0.07 | 0.18 | 0.06 | 0.12 |
| Outer East Siberian Sea | 340,000 km$^2$ | Tg C y$^{-1}$ | 0.20 | 0.31 | 0.62 | 0.23 | 0.39 |
| Total outer shelf area | 620,000 km$^2$ | Tg C y$^{-1}$ | 0.25 | 0.37 | 0.80 | 0.29 | 0.51 |

1033
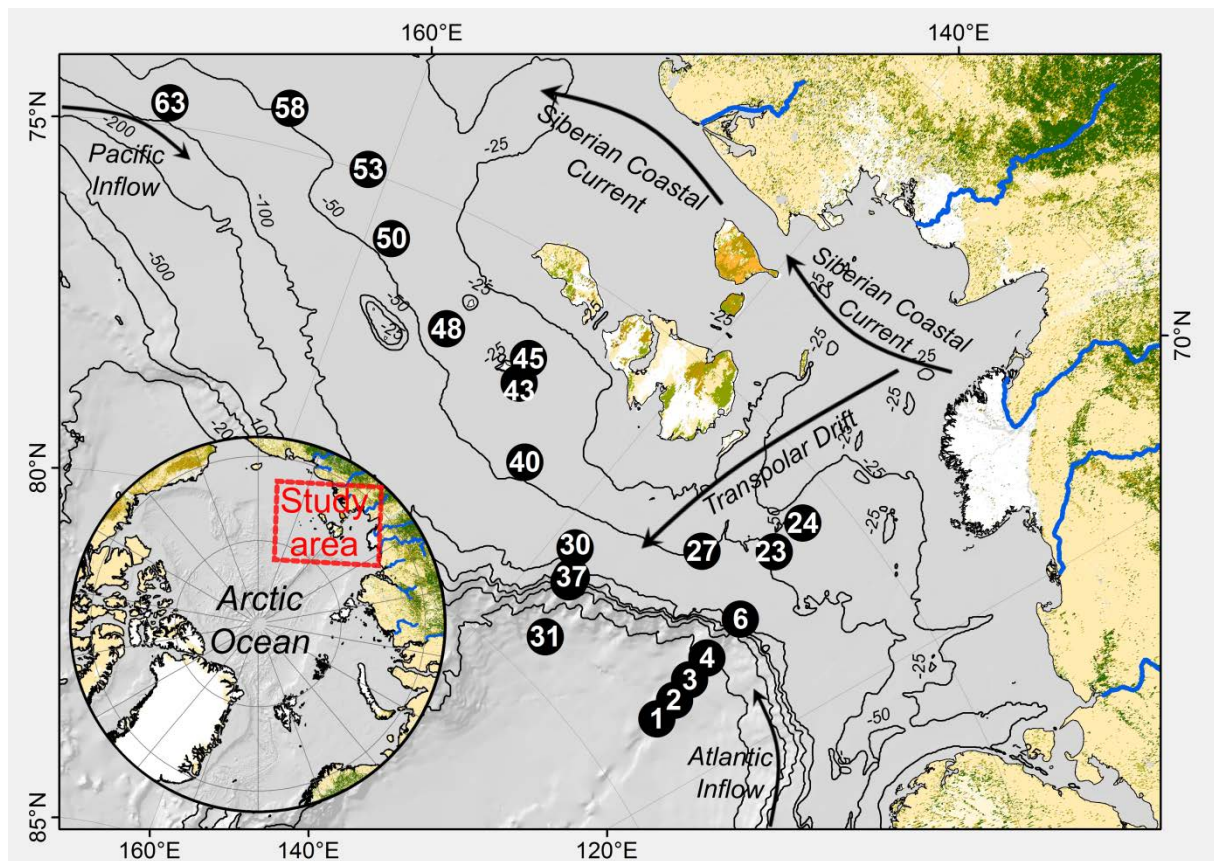
1034    Fig. 1. Map of the Eastern Siberian Sea and slope and station locations.

1035

1036
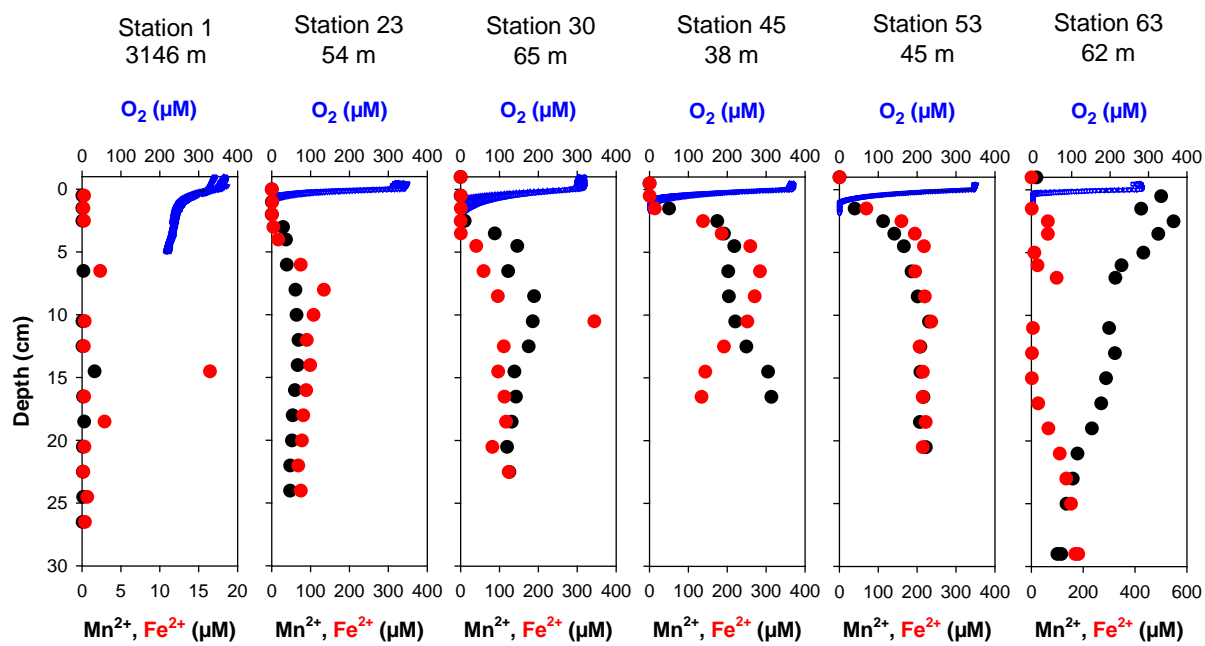
1037

1038     Fig. 2. Depth profiles of dissolved $O_2$, $Fe^{2+}$, and $Mn^{2+}$ at Stations 1, 23, 30, 45, 53, and 63. For

1039     microelectrode profiles, 4 replicates are shown for each station. Depth resolution of measurement

1040     for $O_2$ was 100 μm.

1041

1042

1043

1044
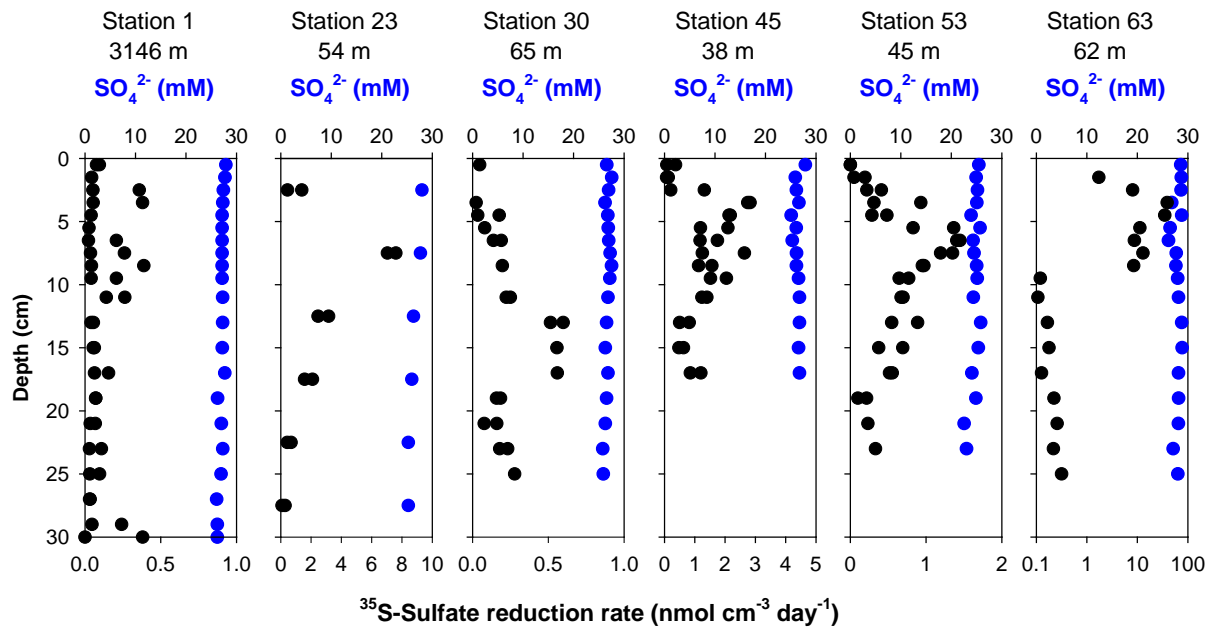
1045

1046 Fig. 3. Depth of profiles of ^{35}S-sulfate reduction rates and porewater concentration of dissolved
1047 sulfate for Stations 1, 23, 30, 45, 53, and 63. Replicate incubation was conducted for each depth
1048 except for Station 63.

1049
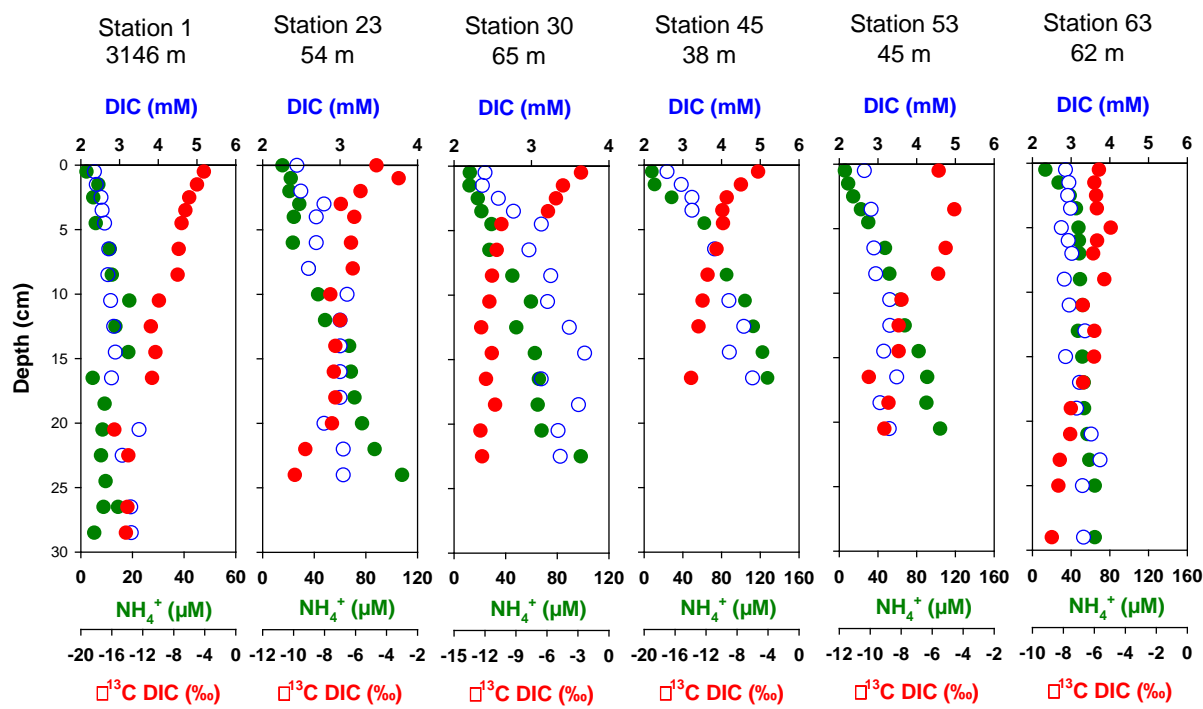
1052 Fig. 4. Depth profiles of porewater dissovled inorganic carbon (DIC), $\delta^{13}$C DIC and porewater $NH_4^+$ at
1053 stations 1, 23, 30, 45, 53, and 63.

1054

1055
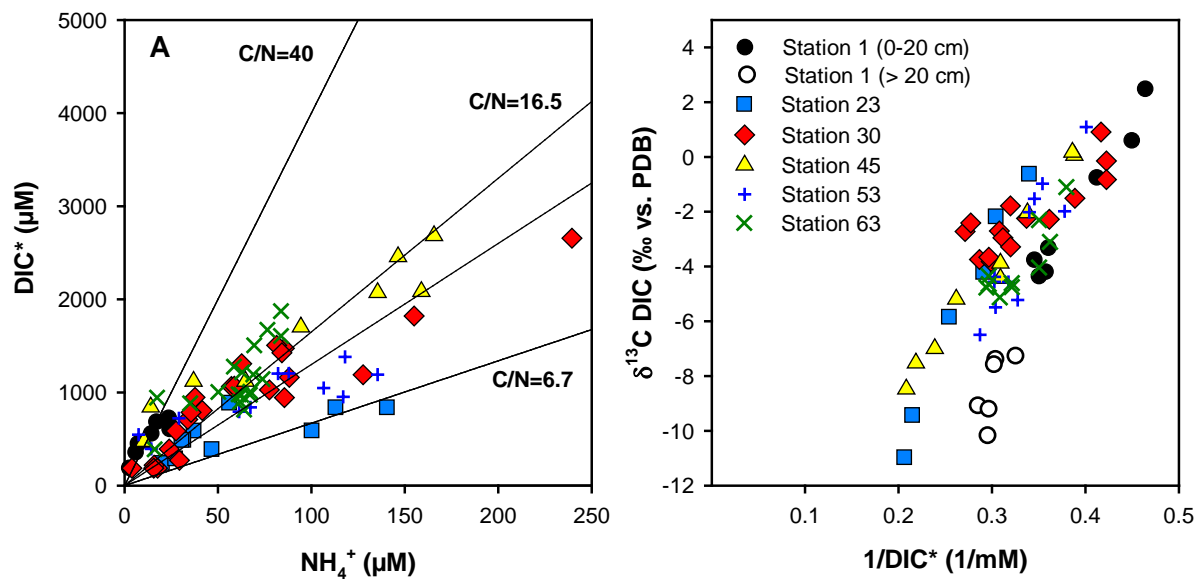
1056

1057 Fig. 5. A: Crossplot of dissolved $NH_4^+$ and porewater DIC* after correction for bottom water DIC
1058 concentrations. The slopes of the regression lines for the individual stations are shown in Table 2. B:
1059 Keeling plot of the fraction of remineralized DIC calculated from a 2-endmember mixing model
1060 versus $\delta^{13}$C DIC.

1061

1062
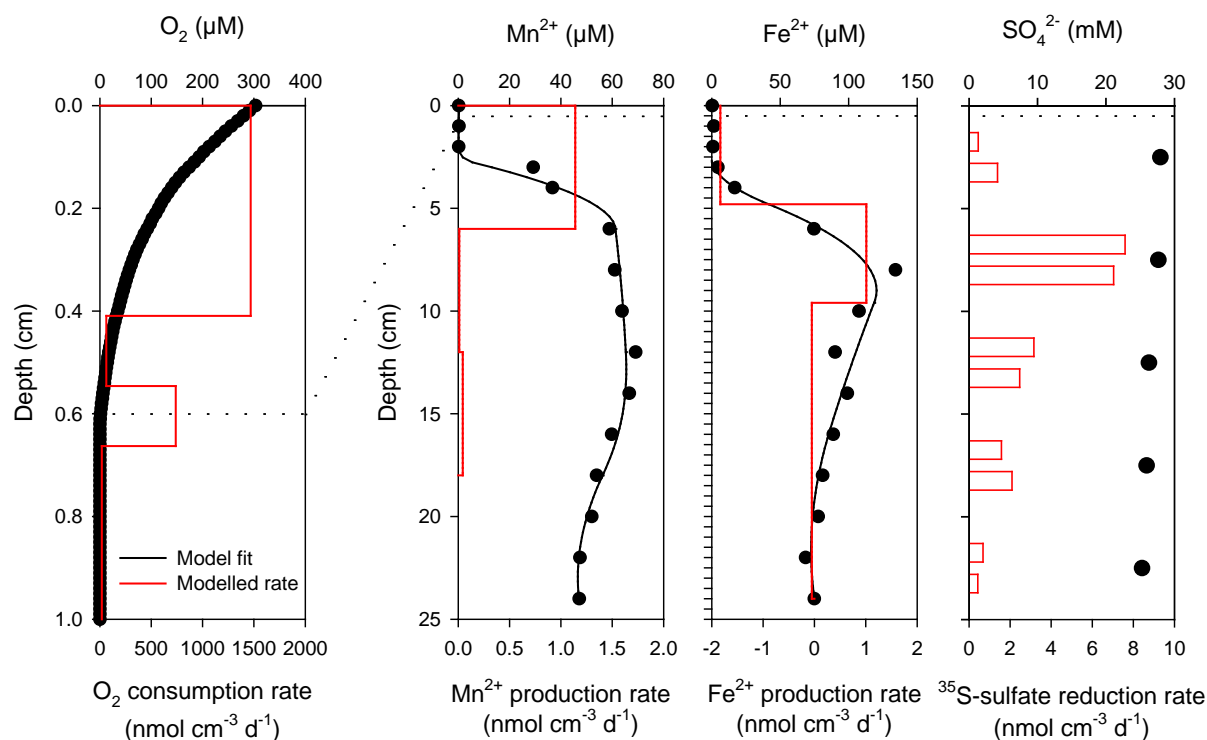
1063

1064    Fig. 6.  Comparison of reaction rates of oxygen, manganese, iron, and sulfate reduction at Station 23.

1065    Note the different depth scale for the $O_2$ consumption rate. The dashed line marks the oxygen

1066    penetration depth.

1067

1068
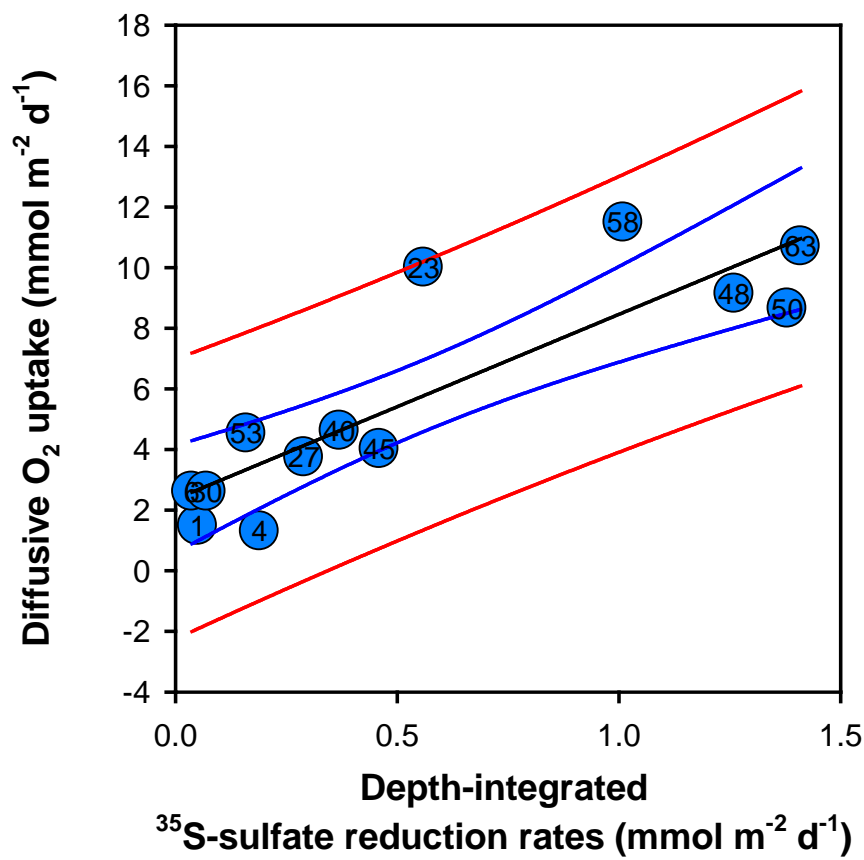
1069

1070     Fig. 7. Crossplot of diffusive oxygen uptake and integrated sulfate reduction rates. The black line is

1071     the linear regression and yielded a y-intercept of 2.1 mmol m$^{-2}$ d$^{-1}$ and a slope of 6.1 ± 0.1. Blue and

1072     red lines show the 95% and 99% confidence interval.

1073

1074

1075
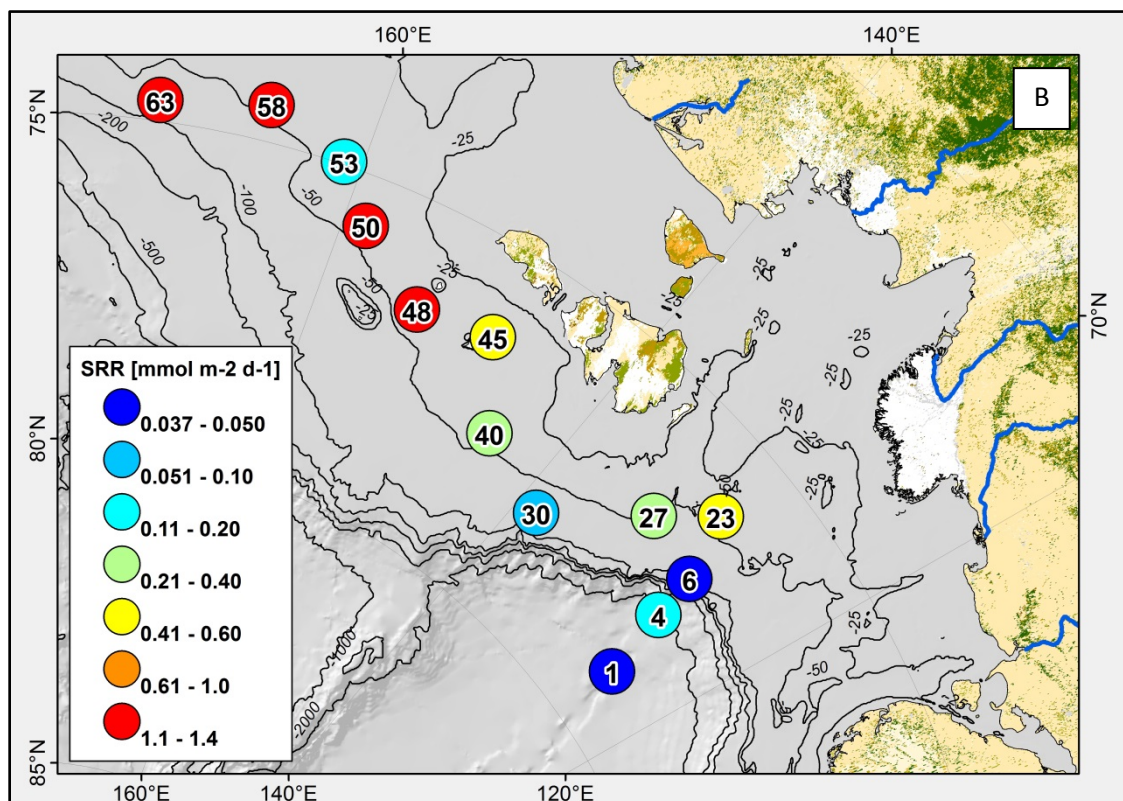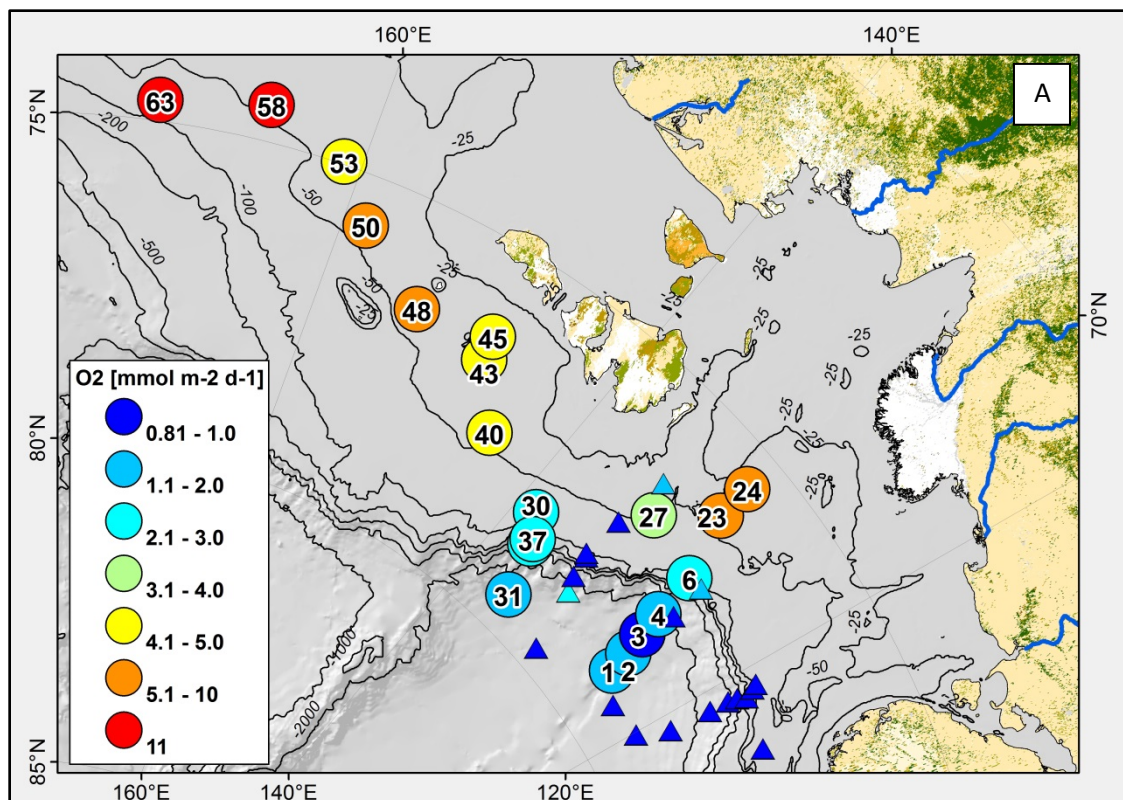
Fig. 8 A, B. Map of field area and sampling stations showing oxygen uptake rates in panel A and
depth-integrated sulfate reduction rates in panel B.

1076

1077

1078

1079
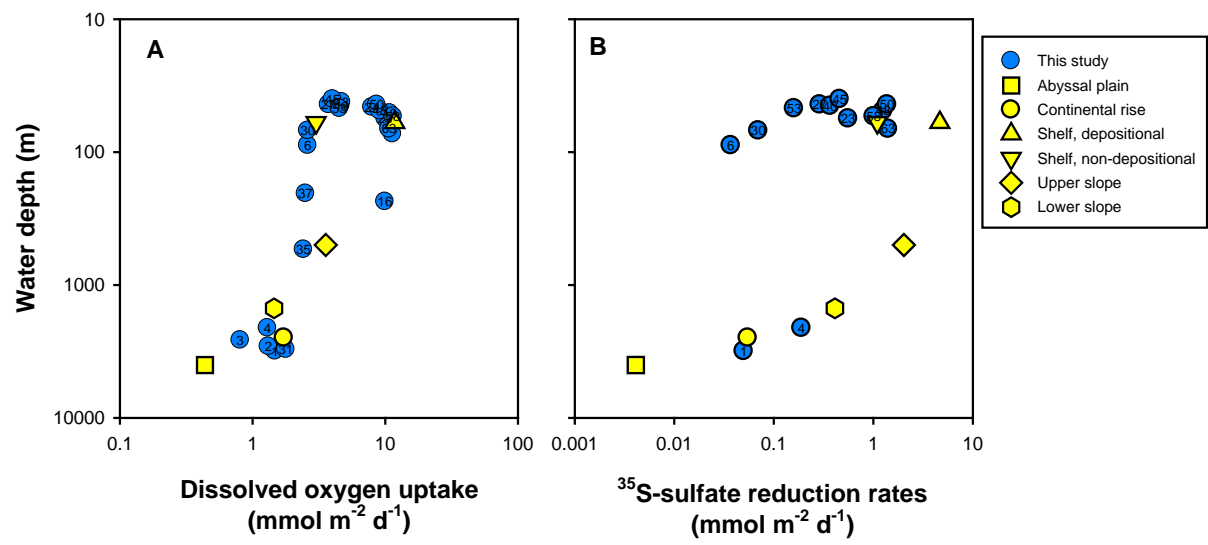
1080

1081 Fig. 9A. Water depth variation of sediment oxygen uptake. 9B: Water depth variation of integrated

1082 $^{35}$S-sulfate reduction rates (0-30 cm sediment depth). For reference average rates of abyssal plain,

1083 continental rise, slope, and shelf sediments, deposition and non-depositional from Canfield et al.

1084 (2005).

1085